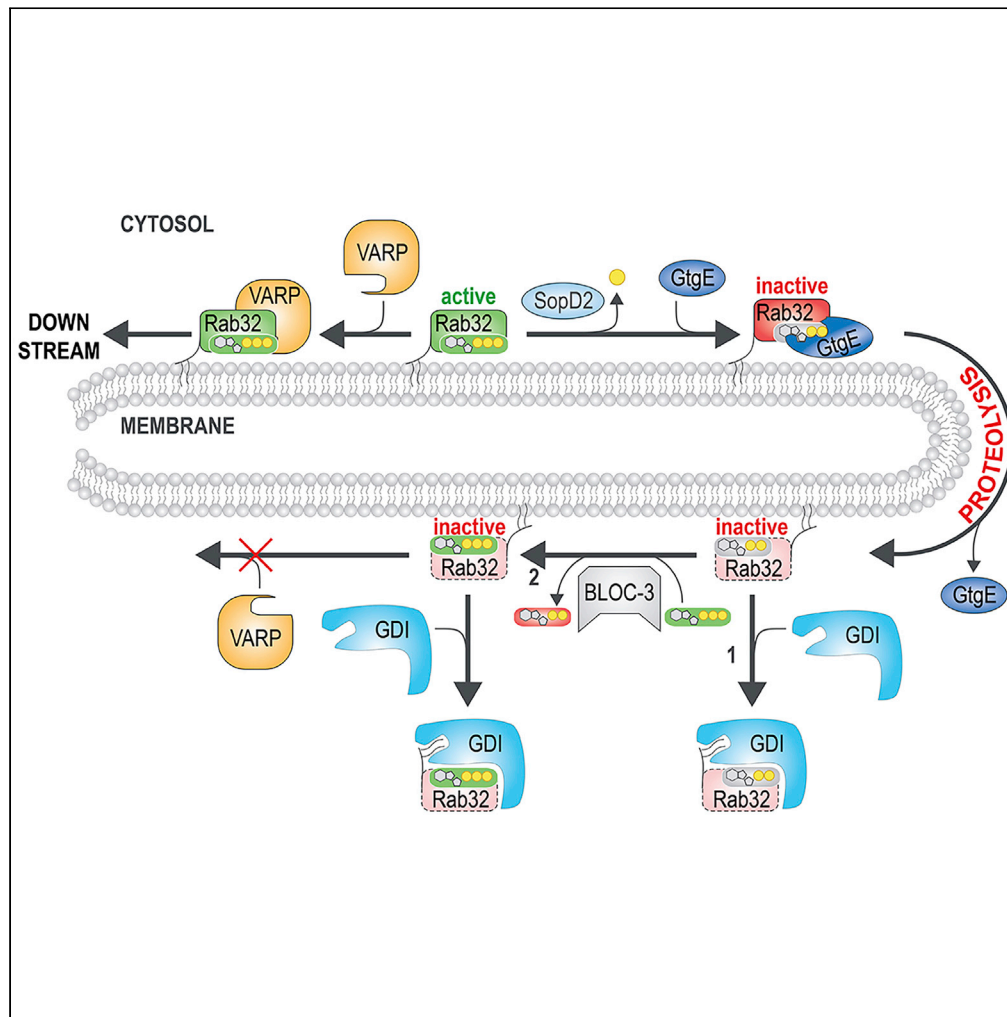# iScience

Article

Proteolysis of Rab32 by *Salmonella* GtgE induces an inactive GTPase conformation

Sergey Savitskiy,
Rudolf Wachtel,
Danial Pourjafar-
Dehkordi, ...,
Michael Sattler,
Martin Zacharias,
Aymelt Itzen

a.itzen@uke.de

Highlights

Cleavage by GtgE disrupts Rab32 interswitch region and blunts its binding to VARP

Cleaved Rab32 can bind GDI in both nucleotide states

Proteolytic PTM of Rab32 results in increased flexibility of the switch regions

Proteolysis forces Rab32 to its inactive structural state even upon GTP binding

Article

Proteolysis of Rab32 by *Salmonella* GtgE induces an inactive GTPase conformation

Sergey Savitskiy,[1,2] Rudolf Wachtel,[2] Danial Pourjafar-Dehkordi,[3] Hyun-Seo Kang,[4,5] Vanessa Trauschke,[6] Don C. Lamb,[6] Michael Sattler,[4,5] Martin Zacharias,[3] and Aymelt Itzen[1,2,7,8,*]

Summary

Rab GTPases are central regulators of intracellular vesicular trafficking. They are frequently targeted by bacterial pathogens through post-translational modifications. *Salmonella typhimurium* secretes the cysteine protease GtgE during infection, leading to a regioselective proteolytic cleavage of the regulatory switch I loop in the small GTPases of the Rab32 subfamily. Here, using a combination of biochemical methods, molecular dynamics simulations, NMR spectroscopy, and single-pair Förster resonance energy transfer, we demonstrate that the cleavage of Rab32 causes a local increase of conformational flexibility in both switch regions. Cleaved Rab32 maintains its ability to interact with the GDP dissociation inhibitor (GDI). Interestingly, the Rab32 cleavage enables GDI binding also with an active GTP-bound Rab32 *in vitro*. Furthermore, the Rab32 proteolysis provokes disturbance in the interaction with its downstream effector VARP. Thus, the proteolysis of Rab32 is not a globally degradative mechanism but affects various biochemical and structural properties of the GTPase in a diverse manner.

Introduction

Small GTPases act as important players in intracellular signaling in eukaryotes. The binary switching of these proteins is realized by binding to different guanosine nucleotides: in the guanosine diphosphate (GDP) state they are inactive and become active by binding to guanosine triphosphate (GTP). The activation does not occur spontaneously but requires the assistance of guanosine nucleotide exchange factors (GEFs) that exchange the tightly bound GDP with GTP (Vetter and Wittinghofer, 2001). The inactivation is mediated by GTPase-activating proteins (GAPs), which stimulate the intrinsic GTP hydrolysis by accelerating its conversion to GDP and inorganic phosphate (Müller and Goody, 2018).

Among the small GTPases, the family of Rab proteins plays a crucial role in intracellular vesicular trafficking. Rab GTPases are reversibly membrane localized. The membrane localization is typically enabled by virtue of two geranylgeranyl lipids attached post-translationally to their structurally flexible C termini. Membrane delivery and recycling are directly coupled to the activation state of the Rab protein: In the inactive form, Rab proteins are cytosolic as they form a high-affinity complex with the GDP dissociation inhibitor (GDI), which shields the geranylgeranyl lipids in a hydrophobic binding pocket. In the active state, GDI cannot bind to the GTPase, leading to the liberation of the lipids, thereby mediating membrane localization. All interactions of GTPases with downstream effectors are mainly mediated via two conserved sequence regions called switch I and II, respectively (Figure 1A). The switch regions are structurally disordered in the inactive state and adopt a highly ordered structure in the active state due to the interactions of the GTP γ-phosphate with both regions (Vetter and Wittinghofer, 2001; Müller and Goody, 2018).

Many bacterial pathogens are taken up by human immune cells via phagocytosis and can survive inside the host. As human cells possess elaborate defense strategies against bacteria, the intruders have evolved strategies to manipulate signaling pathways of the host cell to their advantage. As Rab proteins control vesicular trafficking events (e.g., endosome fusion with lysosomes (Bucci et al., 2000)) that can lead to bacterial cleansing, they are particularly often targeted by bacterial enzymes or effectors (Müller et al., 2010; Spanò et al., 2011). A *Salmonella* infection caused by *S. enterica ssp. typhimurium* (*S. typhimurium*) can lead to the nonlethal but common salmonellosis (Crum-Cianflone, 2008). During infection,

[1]Department of Biochemistry and Signaltransduction, University Medical Centre Hamburg-Eppendorf (UKE), Martinistrasse 52, 20246 Hamburg, Germany

[2]Center for Integrated Protein Science Munich (CIPSM), Department Chemistry, Technical University of Munich, Lichtenbergstrasse 4, 85748 Garching, Germany

[3]Physics Department T38, Technical University of Munich, James-Franck-Strasse 1, 85748 Garching, Germany

[4]Institute of Structural Biology, Helmholtz Zentrum München, 85764 Neuherberg, Germany

[5]Chemistry Department, Biomolecular NMR and Center for Integrated Protein Science Munich, Technical University of Munich, 85748 Garching, Germany

[6]Department of Chemistry, Center for Nanoscience (CeNS), NanoSystems Initiative Munich (NIM) and Center for Integrated Protein Science Munich (CIPSM), Ludwig Maximilians-Universität München, Munich Germany

[7]Centre for Structural Systems Biology (CSSB), University Medical Centre Hamburg-Eppendorf (UKE), Hamburg, Germany

[8]Lead contact

*Correspondence: a.itzen@uke.de

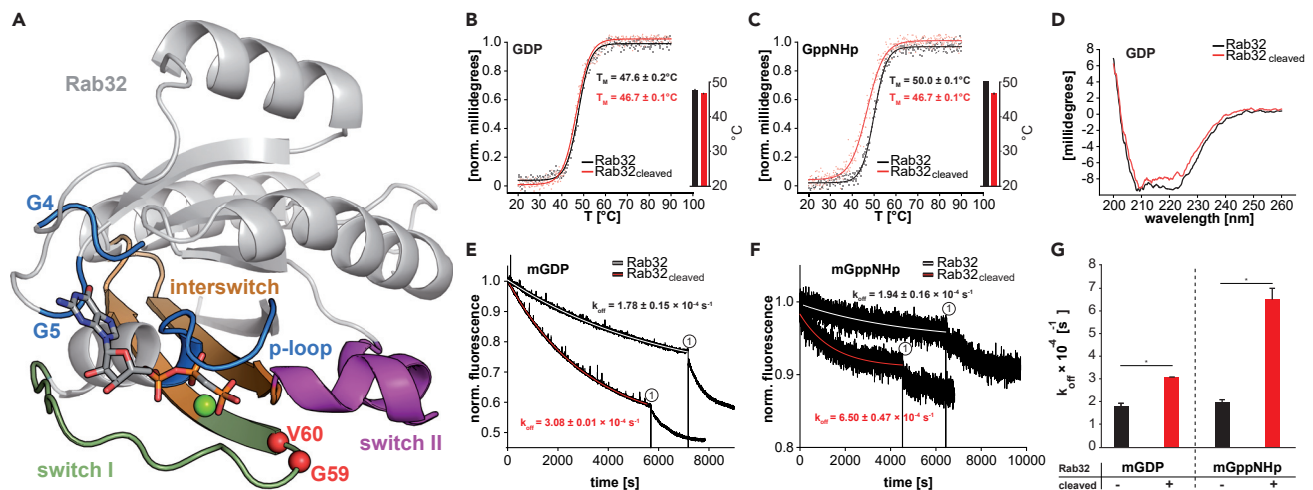https://doi.org/10.1016/j.isci.2020.101940

Figure 1. Biochemical and biophysical characterization of non-modified and cleaved Rab32 in both the activated and inactive states

(A) The crystal structure of Rab32 (4CYM, Hesketh et al., 2014) in the active state is depicted with important structural regions highlighted: switch I (green), switch II (magenta), interswitch region (orange), and P loop, G4, and G5 (blue). GtgE-mediated cleavage occurs between G59 and V60 (red spheres). A non-hydrolyzable GTP analog (GppCp) is represented with sticks. The green sphere represents a magnesium cation.

(B) GtgE-mediated proteolysis does not significantly impact the thermal stability of Rab32:GDP. Left: Normalized thermal unfolding curves of cleaved and uncleaved Rab32:GDP monitored via CD spectroscopy at 220 nm are plotted. The data are fitted with a Boltzmann function yielding the corresponding melting temperature (T_M). Right: Comparison of T_M in both modification states using a bar graph representation. The data are presented as mean $\pm$ SEM (n = 2).

(C) The thermal stability of Rab32:GppNHp is decreased upon GtgE-mediated proteolysis. Left: Normalized thermal unfolding curves of cleaved and uncleaved Rab32:GppNHp monitored via CD spectroscopy at 220 nm are plotted. The data are fitted with a Boltzmann function yielding the corresponding melting temperature (T_M). Right: Comparison of T_M in both modification states using a bar graph representation. The data are presented as mean $\pm$ SEM (n = 2).

(D) The CD spectra of uncleaved and cleaved Rab32:GDP. A comparison does not reveal any global structural differences.

(E and F) mantGDP (E) and mantGppNHp (F) dissociation from Rab32 is elevated in the cleaved state. Mant fluorescence is shown as a function of time and decreases due to nucleotide release of mGDP (0.5 μM Rab32:mGDP, E) or mGppNHp (0.5 μM Rab32:mGppNHp) induced after the addition (at the time point 0) of a high concentration of non-fluorescent GDP or GppNHp (200 μM), respectively. The addition of 5 mM EDTA (1) maximizes the nucleotide release and leads to full dissociation of the mant-nucleotide. The fluorescence intensity and the time axis were normalized to the start of the reaction.

(G) Quantification of nucleotide dissociation from uncleaved and cleaved Rab32 in both the activated and inactive states (data from E and F) are plotted in a bar graph. The data are presented as mean $\pm$ SEM (n = 3); *p < 0.05.

S. typhimurium secretes (in addition to other effectors) the cysteine protease GtgE via a type III secretion system into the cytosol of the host cell. GtgE targets the GTPase Rab32 subfamily, with Rab32 as the presumed main target (Spanò and Galán, 2012). This results in the proteolytic modification of switch I between G59 and V60 in Rab32, which was found to happen exclusively on inactive, GDP-bound Rab substrates (Spanò et al., 2011; Wachtel et al., 2018). Proteolysis may irreversibly and permanently inactivate Rab32 thereby preventing further interactions with regulating or interacting proteins. As a consequence, this would interfere with the delivery of antimicrobial factors and thereby support the *Salmonella* infection.

Rab32 has multiple functions in the cell. It is involved in the biogenesis of lysosome-related organelles, autophagy, mitochondrial dynamics and regulates phagosome maturation during bacterial invasion (Raposo et al., 2001; Alto et al., 2002; Holt et al., 2006; Wasmeier et al., 2006; Raposo and Marks, 2007; Benado et al., 2009; Bultema et al., 2012; Ao et al., 2014; Haile et al., 2017; Rybnicek et al., 2018; Hu et al., 2019). Moreover, in a recent study, Rab32 has been shown to facilitate the delivery of itaconate, a mitochondrial metabolite with antimicrobial activity, into the *Salmonella*-containing vacuoles (SCVs), thereby restricting the replication of *Salmonella* (Chen et al., 2020). To fulfill its functions, Rab32 must cycle between activity states. Thus, Rab32 is activated by the GEF BLOC-3 and can promote intracellular vesicular trafficking by binding to its effector protein VARP (Tamura et al., 2009; Gerondopoulos et al., 2012; Hesketh et al., 2014). Its inactivation can be mediated by its physiological GAP RUTBC1 or the bacterial effector SopD2 from *Salmonella* (Nottingham et al., 2011; Marubashi et al., 2016; Spanò et al., 2016).

The structural basis of the Rab32-GtgE interaction has been reported recently (Wachtel et al., 2018). The proteolytic cleavage of Rab32 by GtgE does not lead to protein unfolding, suggesting that the cleaved form of Rab32

(referred to as Rab32$_{cleaved}$) may still be able to function in intracellular signaling (Wachtel et al., 2018). To investigate the molecular consequences of Rab32 cleavage, we conducted detailed biochemical, functional, and structural analyses. We compared the properties of intact Rab32 with Rab32$_{cleaved}$. A combination of molecular dynamics (MD) simulations, nuclear magnetic resonance (NMR) experiments, and single-pair Förster resonance energy transfer (spFRET) analyses revealed an increase in the conformational flexibility of switch I and switch II. Additionally, Rab32$_{cleaved}$ has an altered protein interaction profile, enabling GDI binding to inactive, cleaved Rab32 and fully impairing the Rab32-VARP interaction.

Results

Proteolytic modification of Rab32 affects its nucleotide binding

After GtgE-mediated cleavage of Rab32, the GTPase domain remains a stable and monomeric protein in solution (Wachtel et al., 2018). To dissect the functional consequences of Rab32 cleavage, we conducted detailed biochemical characterizations.

To elucidate if the proteolytic modification destabilizes the GTPase, we individually determined the protein melting temperature (T_M) as a proxy for the stability of intact and cleaved Rab32 in the GTP-bound and GDP-bound states, respectively. Thermal unfolding monitored by the changes in the circular dichroism (CD) of secondary structure elements revealed that GtgE-mediated cleavage of Rab32:GDP causes a non-significant T_M decrease of 0.9°C (from 47.6°C to 46.7°C) (Figure 1B). Furthermore, the nucleotide exchange from GDP to GppNHp (a non-hydrolyzable GTP analog) results in an increased T_M value (50.0°C), which can be explained by the induced conformational order in the switch regions (Milburn et al., 1990). However, this stabilization effect is not reflected in the Rab32$_{cleaved}$:GppNHp melting temperature (Figure 1C). Proteolysis of Rab32:GDP with subsequent nucleotide exchange does not affect the T_M (46.7°C) of either nucleotide states. Overall, the CD studies show that GppNHp has no stabilizing effect on cleaved Rab32 and its switch regions compared with the uncleaved state. Additionally, CD spectroscopy reveals that there are no notable substantial structural changes after GTPase proteolysis (Figure 1D).

Both switch regions contribute to the stabilization of the nucleotide in the nucleotide-binding pocket of small GTPases (Pai et al., 1989; Milburn et al., 1990; Scheidig et al., 1999). Thus, the nucleotide dissociation properties may be used to investigate the impact of GtgE-mediated cleavage on the stability of the switch regions. To investigate the nucleotide dissociation rates, Rab32 was loaded *in vitro* with modified GDP or GppNHp bearing the fluorescent 2′/3′-O-(N-Methyl-anthraniloyl) (mant) moiety attached to the ribose (mGDP or mGppNHp). The nucleotide dissociation was monitored by the decrease in mant fluorescence intensity as a function of time after the addition of an excess amount of non-fluorescent counterparts (GDP or GppNHp). The nucleotide dissociation rate (k_{off}) of the proteolytically cleaved Rab32 increased regardless of the nucleotide state. Rab32:mGDP shows a k_{off} value of $(1.78 \pm 0.15) \times 10^{-4} \, s^{-1}$ for non-modified and $(3.08 \pm 0.01) \times 10^{-4} \, s^{-1}$ for the cleaved state. On the other hand, Rab32:mGppNHp has a k_{off} value of $(1.94 \pm 0.16) \times 10^{-4} \, s^{-1}$ for uncleaved and $(6.50 \pm 0.47) \times 10^{-4} \, s^{-1}$ for the cleaved state (Figures 1E and 1F). Thus, the nucleotide dissociation rate is almost doubled for mGDP or tripled for mGppNHp in cleaved Rab32 (Figure 1G). As GtgE proteolytically cleaves the switch I region, which is involved in nucleotide binding and magnesium ion coordination, it is not surprising that the cleavage leads to an increased nucleotide dissociation rate caused by destabilization of the switch I.

Proteolysis reduces binding of Rab32 to the VARP-ANK1 domain

As proteolysis of Rab32 may affect binding to its effectors, we investigated the interaction between Rab32 and its physiological interaction partners, the ANK1-domain of VARP and GDI. VARP is an effector of Rab32 that specifically binds to the uncleaved active GTPase through its ANK1-domain (Tamura et al., 2009). Assuming the exchange from Rab$_{cleaved}$:GDP to Rab$_{cleaved}$:GTP is not impaired by the proteolytic modification, the interaction with VARP might still be possible. In case the nucleotide exchange is prevented by the cleavage, it would render Rab32$_{cleaved}$:GDP a dead end for the downstream signaling with VARP. However, Rab32$_{cleaved}$:GDP might still be able to bind to GDI. To test both scenarios, we prepared uncleaved and cleaved Rab32 in each activation state *in vitro* and tested their binding capability with VARP and GDI, respectively, via analytical size exclusion chromatography (aSEC) (Figure 2).

As expected, neither Rab:GDP nor its proteolytically modified counterpart form a complex with the VARP-ANK1, whereas Rab32:GppNHp forms a stable complex with the ANK1-domain (Figures 2A and 2B) (Hesketh et al., 2014). However, there is no binding observed between Rab32$_{cleaved}$:GppNHp and
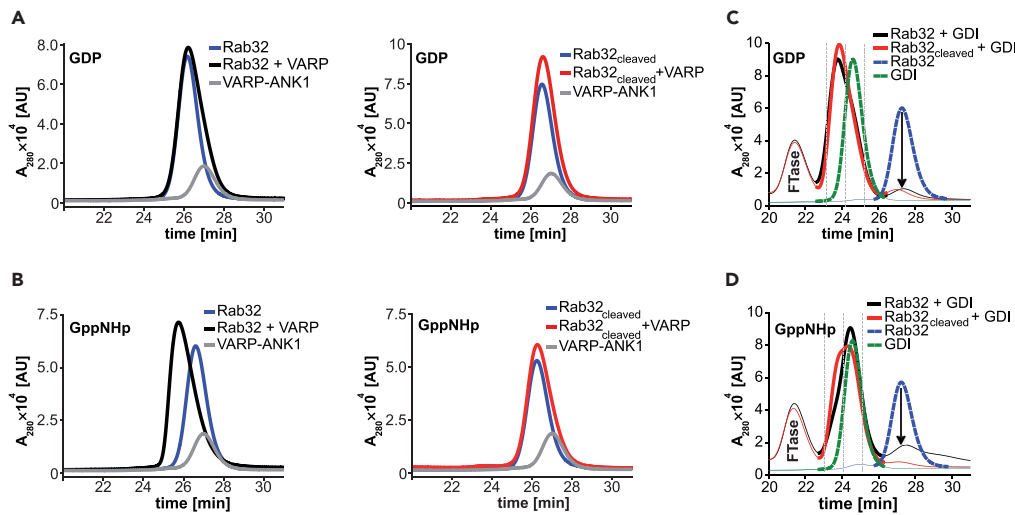
Figure 2. Binding of Rab32 with its physiological interaction partners is selectively impaired by the proteolytic modification

To investigate the interaction of Rab32 with other proteins, aSEC measurements were preformed where the intensity at 280 nm was monitored and the resulting peaks were deconvolved into the individual species.

(A) Left: aSEC measurements of Rab32:GDP in the presence of VARP. VARP-ANK1 does not bind Rab32:GDP *in vitro*. Rab32 (50 μM) was preparatively loaded with GDP (98%) and equilibrated for complex formation with 50 μM VARP-ANK1 for 1 h at 15°C. Subsequently, 50 μL was chromatographically separated via aSEC. The individual runs of single proteins serve as a reference. Right: aSEC measurements of cleaved Rab32:GDP in the presence of VARP. Cleaved Rab32:GDP also does not form a complex with VARP-ANK1.

(B) Left: Complex formation between active Rab32 and VARP-ANK1 investigated using aSEC. The analysis corresponds to that used in (A) starting with Rab32:GppNHp (90% loaded). Here, clear complex formation is observed. Right: aSEC measurement of the interaction between cleaved Rab32:GppNHp and VARP-ANK1. Cleavage of Rab32 impairs the complex formation between Rab32 and VARP-ANK1.

(C) aSEC measurements of the interaction of Rab32:GDP with GDI in the uncleaved and cleaved states. Inactive Rab32 (100% loaded with GDP) binds GDI regardless of the state of its proteolytic modification.

(D) aSEC measurements of the interaction of Rab32:GppNHp with GDI in the uncleaved and cleaved states. Rab32cleaved:GppNHp can more efficiently form a complex with GDI when compared with the uncleaved Rab32. This can be clearly seen in the reduction of the Rab32 only peak for Rab32cleaved:GppNHp when compared with Rab32:GppNHp (arrow); 30 μM B12 was used as internal standard for each aSEC run.

VARP-ANK1 (Figure 2B, left). Thus, the cleavage of Rab32 by GtgE impairs its binding to VARP-ANK1 *in vitro*.

GDI specifically interacts with the inactive state of prenylated Rab GTPases (Sasaki et al., 1990; Wu et al., 2007). The lipid anchor on the C terminus of Rab GTPases is crucial for the interaction with GDI (Wu et al., 2007). To this end, we produced Rab32 bearing the CVIM-sequence on its C terminus for farnesylation (Joberty et al., 1993). Subsequently, it was proteolyzed by catalytic amounts of GtgE, loaded with the desired nucleotide and farnesylated, as described in Transparent methods. Farnesylation was confirmed by mass spectrometry of the intact proteins before and after lipidation (Figure S1). Surprisingly, farnesylated Rab32cleaved:GDP appears to form a complex with GDI, indicated by the reduced elution time of the complex as well as the decreased Rab32 peak (Figures 2C and S2). In contrast to the well-known binding preference of GDI for GDP-bound Rab proteins, the chromatographic data suggest that GDI is also able to form a complex with Rab32cleaved:GppNHp (Figure 2D). Peak decomposition indicates distinct complex formation between GDI and Rab32 in the cases of Rab32:GDP, Rab32cleaved:GDP, and Rab32cleaved:GppNHp (Figure S3). Of note, uncleaved prenylated Rab32:GppNHp seems to form a complex with GDI to some extent (Figure S3). This could be explained by not 100% GppNHp-loaded Rab32 (85% GppNHp). Thus, the resulting complex between Rab32:GppNHp and GDI could be formed by GDP-loaded species present in the sample.

In conclusion, the proteolytic modification of Rab32 results in the disruption of its interaction with VARP-ANK1. Furthermore, the proteolytic cleavage has no effect on the interactions with GDI in the case of Rab32cleaved:GDP; however, in the case of Rab32cleaved:GppNHp, the binding is increased compared with its uncleaved state.
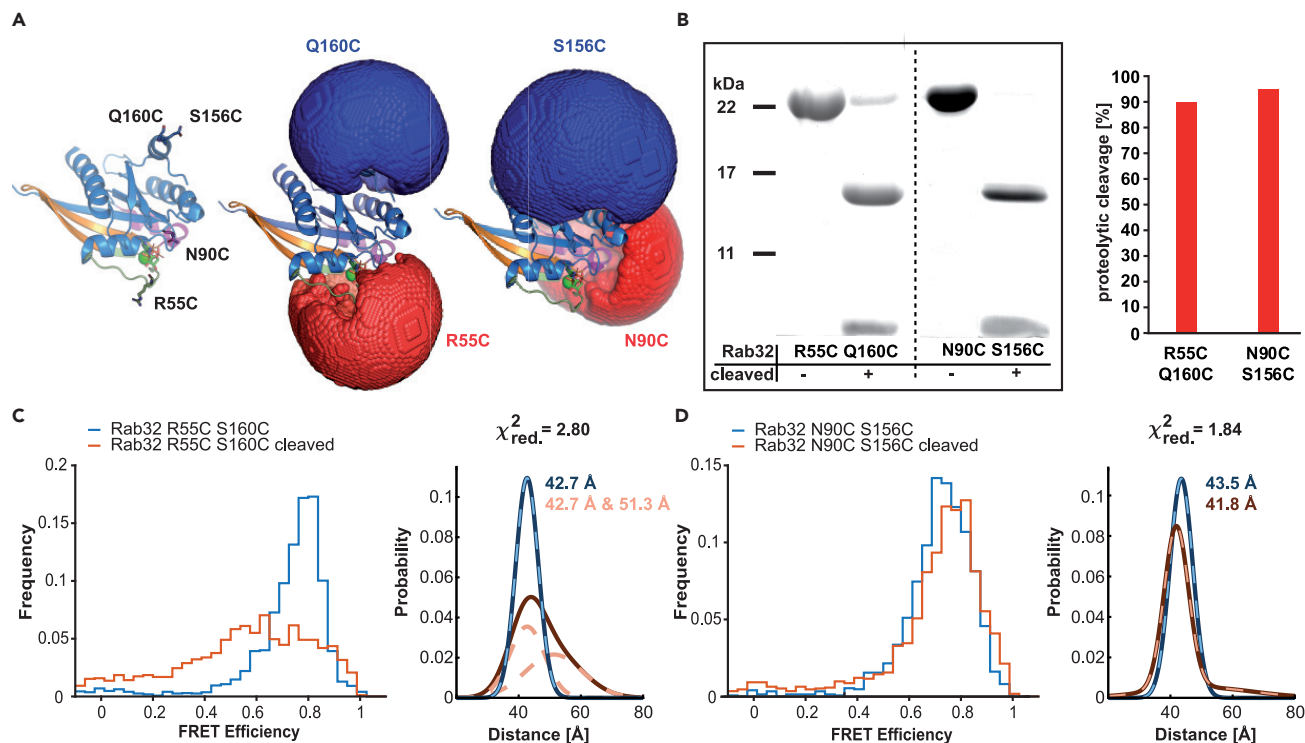
Figure 3. Single-pair FRET reveals changes in the conformation of Rab32 upon proteolytic modification

(A) Position of Cys mutations within the Rab32 for covalent fluorophore linkage. Left: Ribbon structure representation of Rab32 where the selected amino acid positions for protein labeling with FRET pairs are shown as sticks. Middle and right: Visualization of the accessible volume calculations for Rab32$_{R55C\ Q160C}$ and Rab32$_{N90C\ S156C}$ double mutants, respectively. The Rab32 structure used for the current representation is deposited in the PDB under the ID 6FF8 (McGrath et al., 2019).

(B) Quantification of cleavage efficiency for the spFRET Rab32 mutants. Left: Rab32:GDP mutants were proteolytically cleaved and run on an SDS-PAGE gel. Right: Densitometric quantification of the gel bands for modification completion in both double mutants plotted in a bar graph.

(C) SpFRET histograms for the uncleaved and cleaved Rab32$_{R55C\ Q160C}$ mutant revealing a change in distance between fluorophores upon cleavage. The distances calculated using probability distribution analysis approach are indicated. Orange dashed lines show the decomposed peak after proteolysis with two equally populated species.

(D) SpFRET histograms for the uncleaved and cleaved Rab32$_{N90C\ S156C}$ mutant. Cleavage of switch I leads to minor distance differences in the switch II region of the protein. All calculated distances represent the separation of the fluorophores, which are attached to the protein via flexible linkers.

GtgE-mediated cleavage destabilizes switch I and indirectly impacts switch II of Rab32

Next, we investigated the impact of the proteolytic modification in switch I on the conformations of both switch regions of Rab32. To this end, we applied spFRET, which allows the determination of conformational changes within disordered protein regions by detecting distance variations on individual molecules (LeBlanc et al., 2018). Strategically positioned pairs of Cys substitutions within Rab32 served as fluorophore labeling sites. As Rab32 is a small protein, we strived to maximize the distances between the labeling positions on the static portion of the protein (Q160C or S156C) and a potentially dynamic counterpart in either the switch I (R55C) or switch II (N90C) region of the protein (Figure S4). Subsequently, spFRET-suitable fluorophores (Alexa 488-maleimide, Alexa 647-maleimide) bearing a maleimide moiety were covalently coupled to Cys-containing Rab32$_{R55C/Q160C}$ or Rab32$_{N90C/S156C}$ constructs (Figure 3A, left). Intrinsic Cys residues (C145, C162) were mutated to Ser to avoid off-target labeling. The coupled dyes contain flexible linkers not only allowing free rotation but also increasing the volume in which the dye molecule can be located (Table S1). To visualize the spatial distribution of the possible locations of the fluorescent dye, we performed accessible volume calculations that estimate the possible locations of the fluorophore based on its size and the size and length of the linker (Kalinin et al., 2012). Accessible volume calculations for both Rab32 double mutants are presented in Figure 3A. The main goal for the FRET experiments is to detect conformational changes upon cleavage between residues 59 and 60. For this purpose, we also generated pure cleaved Rab32 variants ready for fluorophore labeling and subsequent spFRET measurements (Figure 3B). The proteolytic modification of Rab32$_{R55C/Q160C}$ labeled in switch I generates two species with equal contributions of 50% after peak decomposition (Figure 3C). The distance of

the first species corresponds to uncleaved Rab32, whereas there is an increase in distance of the second species of 8.6 Å between the fluorophores after cleavage (Figure 3C). In the case of the Rab32$_{N90C/S156C}$ labeled in switch II, only minor changes are observed. The cleavage reduces the distance between the fluorophores by ∼2 Å (Figure 3D).

In summary, spFRET data indicate a strong destabilization of the switch I region as well as an indirect minor influence on switch II of Rab32 upon the GtgE-mediated proteolysis.

Rab32$_{cleaved}$:GppNHp exhibits structural similarities with its GDP state

For a better understanding of the structural consequences of GtgE proteolysis in Rab32, NMR studies were conducted (Figures 4 and S5). For this purpose, we recorded and compared ^{1}H, ^{15}N heteronuclear single quantum correlation (HSQC) NMR spectra of the four states (indicated in the schematics in Figure 4B), identifying the effects of GtgE-mediated proteolysis in the presence of different nucleotides (GDP, GppNHp). First, replacement of GDP to GppNHp (non-hydrolyzable GTP analog) in Rab32 shows large spectral differences, where most signals are shifted or broadened in the GppNHp state, that represents the GTP-bound form (Figure 4A, black versus green). This suggests that GTP-induced transition to the active state is not limited to local changes in the switch region, but rather results in a more global conformational change in Rab32. Next, we investigated GtgE-mediated cleavage of Rab32 in the presence of GDP or GppNHp. Upon GtgE-mediated cleavage of Rab32:GDP, a small set of NMR signals is clearly shifted or broadened (Figure 4A, black versus red), likely corresponding to the residues surrounding the cleavage site in the switch region. In contrast, virtually no spectral changes are observed for Rab32:GppNHp upon adding a catalytic amount of GtgE (Figure S5). This indicates that the nucleotide exchange to GppNHp was complete and confirms the preference for GtgE to interact with GDP-bound Rab32 (Wachtel et al., 2018). Last, we tested the effect of GppNHp-binding on the cleaved Rab32:GDP (Rab32$_{cleaved}$:GppNHp). Spectral changes indicate nucleotide exchange from GDP to GppNHp for cleaved Rab32. However, most of the signals do not reach the fully active GppNHp-bound state but rather appear between the two states (Figure 4B, orange box) and are closer to the GDP-bound state (Figure 4B, red box), whereas a few signals of Rab32$_{cleaved}$:GppNHp can be linked to the Rab32:GppNHp state (Figure 4B, green box). In short, the NMR spectral comparisons indicate that (1) GppNHp binding triggers conformational changes beyond the switch region and protects the switch region from proteolysis and (2) GtgE-mediated proteolysis results in local changes in the switch region, which subsequently lock Rab32 in an inactive-like conformational state despite its nucleotide state.

GtgE-mediated cleavage destabilizes the switch regions and disrupts the interswitch region of Rab32

Additionally, we performed MD simulations on cleaved and uncleaved Rab32 in active and non-active conformations. MD simulations are a complementary approach to gain further insights regarding stability and the timescale of the dynamic changes in both switch regions upon the proteolytic modification. Moreover, MD simulations can provide additional structural reasons for the impaired binding between the VARP-ANK1 domain and Rab32$_{cleaved}$:GppNHp.

Simulations were started from the active GTPase conformation with either a bound GDP or GTP and either an intact protein chain or with cleavage between G59 and V60 (see Transparent methods). In the presence of GDP, proteolytic modification leads to a drastically increased root-mean-square deviation (RMSD) of both switch regions in the inactive state of Rab32 relative to the non-modified state, indicating destabilization (Figure 5A). The distributions of the RMSD values demonstrate sampling of conformations for the switch I and switch II regions that deviate from the start structures by ∼16 Å and ∼5 Å, respectively (Figures 5A and 5B right). The following simulations in the presence of bound GTP revealed that GTP binding is not sufficient to maintain the stability and structure of switch I in the cleaved form (Figure 5B, left). Similarly, the RMSD plot in the cleaved state indicates that switch I has higher flexibility compared with its uncleaved state, reaching an RMSD of around 4 Å (Figure 5B, right). However, on the timescale of the simulations, no differences in the flexibility of switch II in case of the cleaved versus uncleaved Rab32 with bound GTP were observed (Figure 5B, right). The simulations indicate that proteolysis of Rab32 disrupts and unfolds the interswitch region of Rab32 independently of its nucleotide-bound state (Figures 5C and 5D, left and middle). This disruption appeared after 500 ns of simulation time and led to the loss of structure of the β2 strand. Moreover, the antiparallel β-sheet strands β2 and β3 drift apart during the simulation (Figures 5C and 5D middle). This is reflected in an increase of the center-of-mass (COM) distance of two residue pairs in the two strands (W80&I82 and V60&F62) observed for both GDP- and GTP-bound cleaved Rab32 in the
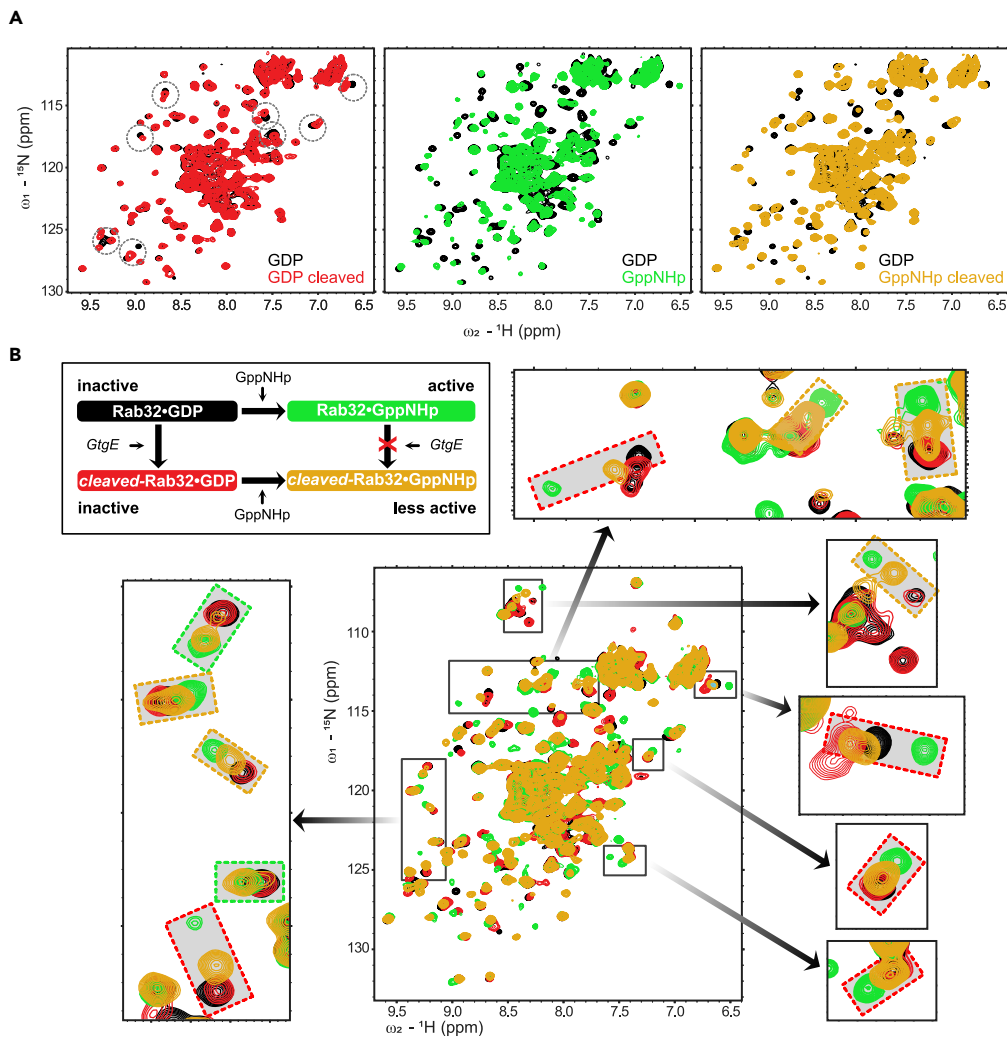
Figure 4. NMR analysis of structural effects of proteolysis and nucleotide binding on Rab32

(A) Superposition of ^{1}H, ^{15}N NMR correlation spectra of ^{15}N-labeled Rab32 with GDP (black) or GppNHp (green) and their cleaved states (red and orange, respectively) by GtgE. Note that the cleaved Rab32:GppNHp (orange) has been produced by proteolysis of Rab32:GDP followed by addition of GppNHp. Specific spectral changes of the GDP state upon cleavage are highlighted with dashed circles.

(B) Summary of the states of Rab32 used for NMR analysis. Spectral overlays of the four states indicate that the NMR signals of the cleaved GppNHp-bound state (orange) generally are more similar to the inactive state (black, red), where the cleaved GppNHp-bound state signals (orange) appear close to the inactive state (red boxes) or intermediate (orange boxes) between the GppNHp-bound active (green) and GDP-bound (black) states. The NMR signals with the cleaved GppNHp-bound state (orange) that correlate with the active state (green) are shown in green boxes.

course of the simulations (see Figures 5C and 5D, right). The local increase in flexibility of the switch regions and unfolding of the interswitch region in cleaved Rab32 observed in the MD simulations is consistent with the spFRET and NMR results, whereas the dissociation of the β2 strand appears not to be reflected in the NMR spectra. Hence, the MD simulations indicate qualitatively the enhanced mobility of the switch and interswitch regions in Rab32 due to cleavage in good agreement with the spFRET and NMR results, but appear to overestimate the effect of cleavage on the β2 strand mobility. Nevertheless, the observed destabilization of the switch regions and unfolded interswitch region of cleaved Rab32 during the simulations explains the reduced interaction of cleaved Rab32 with VARP-ANK1. Both switches and the interswitch region are at the interface in the complex with VARP-ANK1. Consequently, consistent with spFRET data, MD simulations show that proteolysis significantly destabilizes switch I as well as slightly impacts the conformation of switch II. Furthermore, the interswitch region of Rab32 is dramatically disordered independently of
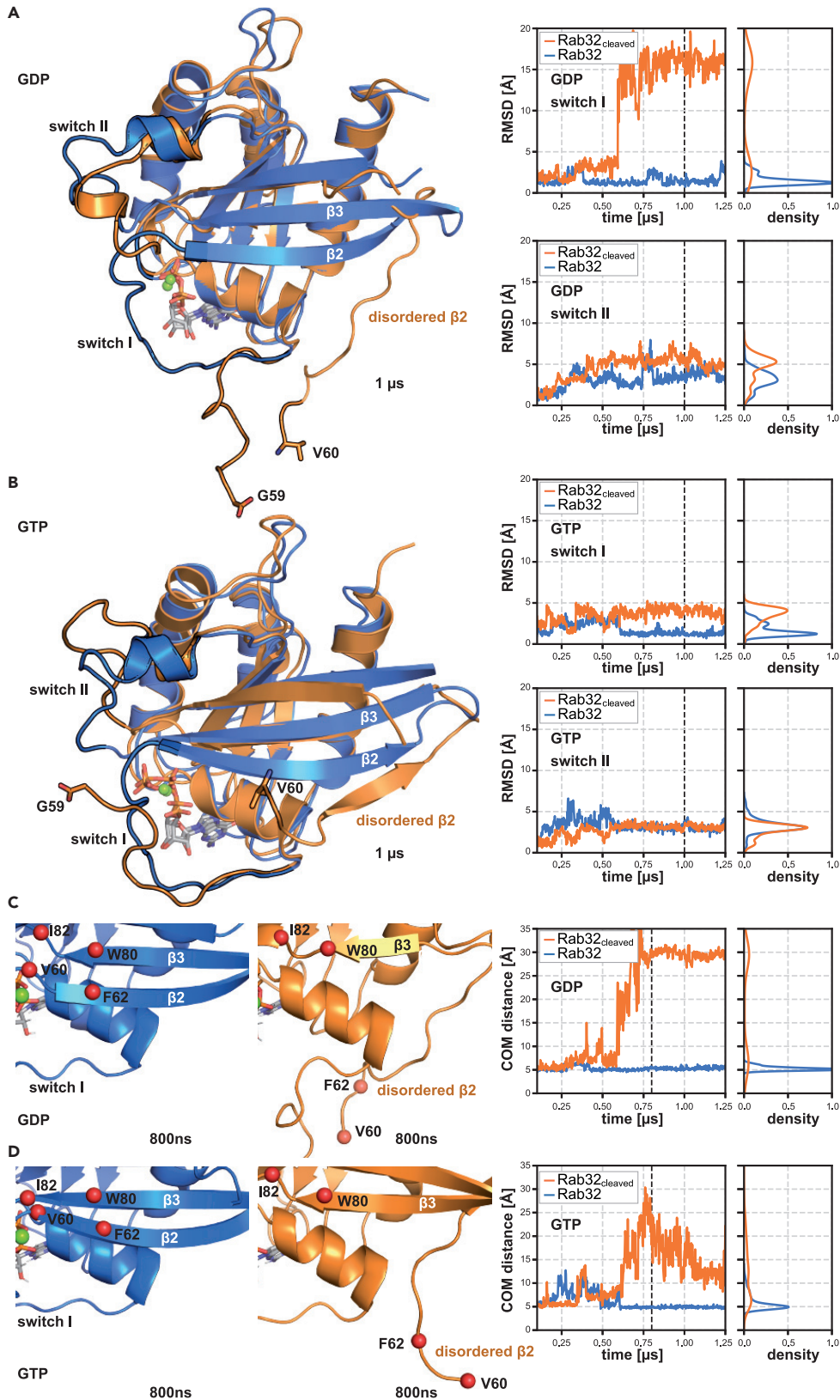
Figure 5. Cleavage-induced flexibility in the switch I promotes unfolding of the β2-strand in the interswitch region of Rab32 (revealed by molecular dynamics simulations)

(A) Left: Superimposed MD simulated structures of Rab32:GDP (blue) and Rab32$_{cleaved}$:GDP (orange, the disordered β2-strand is indicated) after 1 μs of MD simulations. The switch regions are highlighted with black outline. Right: RMSD versus simulation time for switch I and II regions of Rab32:GDP and Rab32$_{cleaved}$:GDP. The black dashed lines indicate the sampling time of the corresponding snapshots shown on the right.

(B) Left: Superimposed MD simulated structures of Rab32:GTP (blue) and Rab32$_{cleaved}$:GTP (orange) after 1 μs. Right: Same as in (A) for the Rab32:GTP and Rab32$_{cleaved}$:GTP.

(C) Left and middle: The interswitch region of Rab32:GDP (blue) and Rab32$_{cleaved}$:GDP (orange) presents the β2 strand at 800 ns of the MD simulation with a large change of the COM (center-of-mass) distances of V60 & F62 and W80 & I82 in the cleaved versus uncleaved states. Red spheres indicate the C$_\alpha$-atoms of the amino acids V60, F62, W80, and I82. Right: V60 & F62 - W80 & I82 COM distances versus simulation time. The point of 800 ns, indicated by the black dashed line, highlights the time point of the snapshots shown in the left and middle panels.

(D) Same as in (C) but for the versus Rab32:GTP case.

its nucleotide state upon proteolysis. Both switches and the interswitch region are at the interface in the complex with VARP-ANK1 domain explaining the reduced interaction of cleaved Rab32 with VARP-ANK1.

Discussion

In this study, we present structural and biochemical investigations on the consequences of GtgE-mediated cleavage of inactive Rab32. Our findings show that the proteolytic modification of switch I does not affect the global structural stability of the protein but leads to local changes of the structure and destabilization of switch I and switch II. Moreover, the regioselective cleavage of switch I disrupts the interswitch region of Rab32 leading to unfolding of the β-sheet structure of the β2 strand. Moreover, Rab32$_{cleaved}$:GppNHp is not able to interact with its effector VARP-ANK1. In contrast, proteolysis does not impair the interaction between Rab32:GDP and GDI. Furthermore, Rab32$_{cleaved}$:GppNHp but not Rab32:GppNHp is able to bind to GDI.

Amino acid residues from switch I (V60, D61, and F62), switch II (M91, V94, R93, Y95, and K97) and the interswitch region (D61, L64, and W80) are crucial to establishing an interaction surface between Rab32 and VARP-ANK1 (Figures 6A and 6B) (Hesketh et al., 2014). Interestingly, the Met and Arg residues from switch II, which correspond to positions 91 and 93 in Rab32, respectively, are conserved only in the Rab32 subfamily and are vital for the interaction with the ankyrin repeats (Hesketh et al., 2014; Purlyte et al., 2018). The importance of the interswitch region of small GTPases for the interaction with their effectors has been reported previously (Zhu et al., 2004; Eathiraj et al., 2005, 2006; Wu et al., 2005; Jagoe et al., 2006). Likely, the gain in structural flexibility of the switch regions of cleaved Rab32 accompanied by interswitch unfolding indicated by spFRET data and MD simulations lead to a disturbance of the interaction between Rab32$_{cleaved}$:GppNHp and its effector. Additionally, proteolytic modification of Rab32 forces β2 and β3 strands to drift apart, as indicated by the increased COM distances between these two β strands in the MD simulations. This, in turn, displaces all residues of the β2 strand involved in the interaction with VARP-ANK1 and, in this fashion, contributes to break down of the Rab32:VARP-ANK1 interaction. VARP participates in trafficking of melanogenic enzymes and has been suggested to control the transport in the endosome-to-cell surface route by regulating the activity of retromer (Tamura et al., 2009, 2011; Hesketh et al., 2014; Marubashi et al., 2016). However, the role of Rab32 as a binding partner of VARP is not entirely understood (Hesketh et al., 2014). The destruction of the interaction between Rab32 and VARP may lead to a missorting and degradation of melanogenic enzymes or disruption of trafficking out of the endosome in the cell periphery (Tamura et al., 2009, 2011; Bultema et al., 2012; Hesketh et al., 2014; Marubashi et al., 2016).

Moreover, a recent study has shown that proteolytic modification of the switch I in KRas by the Ras- and Rap1-specific protease (RRSP) from *Vibrio vulnificus*, analogous to the activity of GtgE in Rab32, impairs the binding to its interaction partner RAF (Biancucci et al., 2018). In contrast to GtgE, RRSP cleaves switch I of KRas in its middle and not near its C-terminal end. Analogous to GtgE-mediated proteolysis, cleavage by RRSP impacts the β2 strand of KRas (Biancucci et al., 2018). However, Rab32 and KRas differ in the nucleotide binding properties after proteolytic modification: Cleaved Rab32 but not KRas shows elevated GDP/GTP dissociation rates. Stable nucleotide binding in KRas is assumed to be ensured by F28 binding to the guanine moiety, but the identically positioned F50 in Rab32 is not sufficient for nucleotide stabilization after GtgE-mediated proteolysis (Biancucci et al., 2018). Additionally, the results of our spFRET experiments and MD simulations show that switch I gains structural flexibility after proteolysis and thus likely does not contribute to the stabilization of the nucleotide in its binding pocket. The existence of two species of cleaved Rab32$_{R55C/Q160C}$, as demonstrated
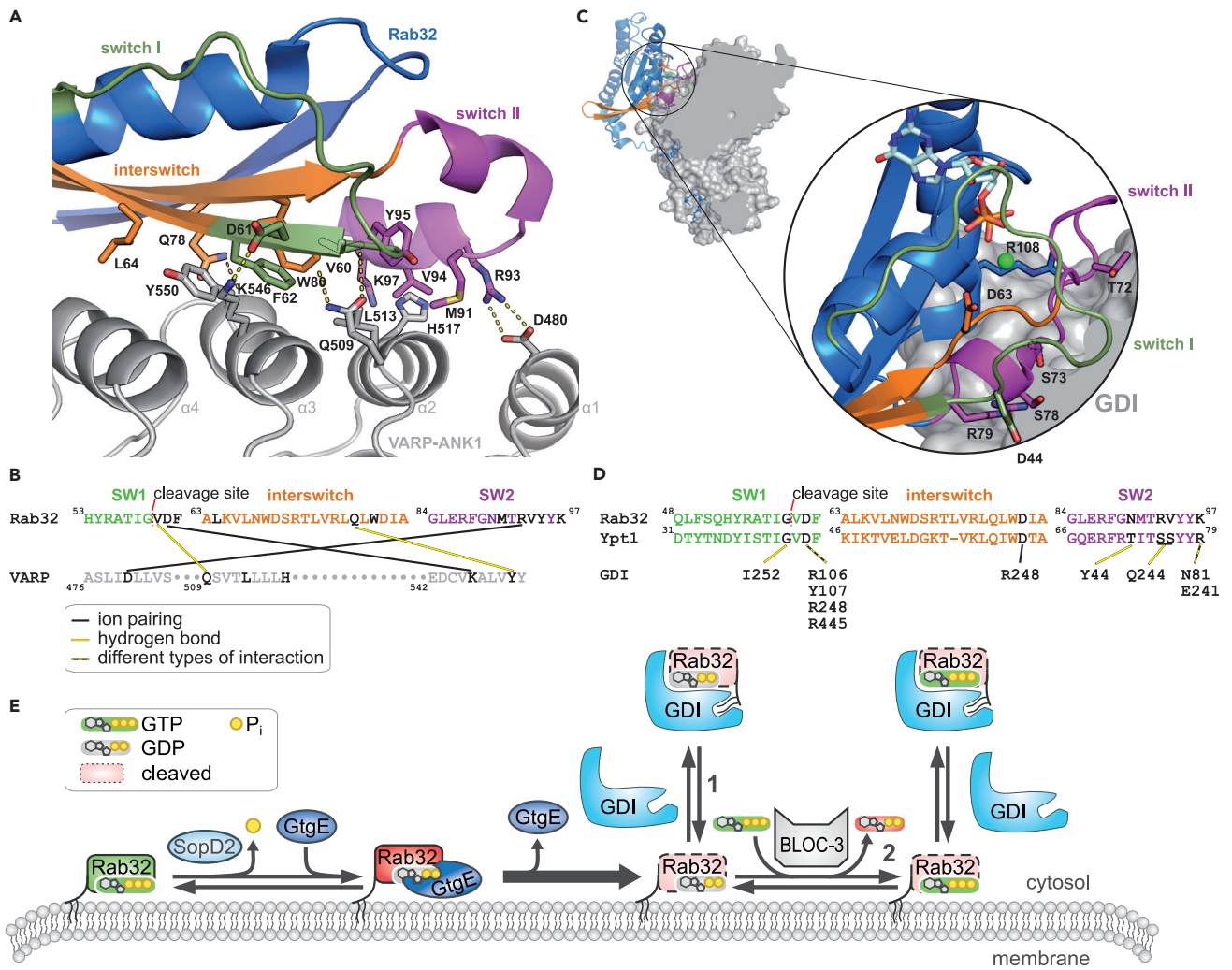
Figure 6. Models of the molecular basis for binding effects of cleaved Rab32 with its interaction partners

(A) Structural representation of Rab32 (colored) and VARP-ANK1 (gray) with important interaction residues presented as sticks (PDB: 4CYM, Hesketh et al., 2014).

(B) The sequence of the switch I, switch II, and interswitch region of Rab32 with corresponding interacting amino acids from VARP-ANK1 depicted in black. Salt bridges between amino acids are indicated by black-yellow lines.

(C) A structural representation of Ypt1 (yeast GTPase) and GDI showing the interaction surface and important interaction residues of switch I, switch II, the interswitch region, and the C-terminal region of Ypt1 with hydrophobic moiety (PDB: 2BCG, Pylypenko et al., 2006). Structural representations of the proteins were prepared using PyMol.

(D) Sequence comparison of the GDI-interacting regions of Ypt1 and Rab32 with crucial amino acids for the GDI binding depicted in black. Amino acids contributing to the interaction between the two protein structures are shown in black.

(E) Model of the hypothetical life cycle of Rab32 during the *Salmonella* infection process with possible routes for proteolyzed Rab32. Once the intrinsic hydrolysis of GTP to GDP occurs in Rab32, which is accelerated by SopD2 from *Salmonella*, it can be processed by GtgE protease and take one of two possible pathways, indicated with arrows 1 or 2, respectively.

by two different distances between the fluorophores from the spFRET measurements, could be explained by dynamic behavior of the proteolyzed switch I region. Thus, switch I of Rab32$_{cleaved}$ is not displaced from the protein core permanently, but attaches and detaches dynamically. Therefore, the position of the cleavage site within switch I plays an important role in its conformational stability and the nucleotide-binding ability.

Changes in the Rab32 structure caused by proteolysis are not enough to impair the interaction with GDI. Comparing Rab32 with Ypt1 in complex with GDI, G59, and D61 from switch I; N90, R93, V94, and K97 from switch II; and only D81 from the interswitch region contributes to the Rab32:GDI complex formation (Figures

6C and 6D) (Pylypenko et al., 2006). As the proteolytic modification has an immense influence on the localization of the interswitch region and switch I, they are apparently not vital for the interaction with GDI. Therefore, the Rab32 binding to GDI is presumably determined by the structural organization of switch II. Noteworthy, bulky post-translational modifications on switch II (such as AMPylation, enzymatic transfer of AMP moiety to a target molecule) of Rab1b impair the interaction with GDI (Goody et al., 2012; Oesterlin et al., 2012; Levin et al., 2016). Nonetheless, the indirect minor impact of GtgE-mediated cleavage on the switch II has a big consequence for the interaction of Rab32 with GDI resulting in the ability to bind to $Rab32_{cleaved}$:GDP and $Rab32_{cleaved}$:GTP. Recently, it has been shown that bacteria can lock Rab1b in the active state using AMPylation (Barthelmes et al., 2020). Consequently, *Salmonella* may use proteolysis to force Rab32 into an inactive-like conformation as demonstrated here by NMR. This may explain the ability of $Rab32_{cleaved}$ to interact with GDI in the GDP and GTP states.

Once proteolyzed, cellular Rab32-signalling could hypothetically develop in two ways: (1) immediate interaction with GDI and withdrawal from the membrane or (2) GEF-mediated nucleotide exchange to GTP followed again by GDI interaction and withdrawal from the membrane (Figure 6E). The first route seems to be adequate, whereas the second one is questionable, as Rab32 must be first activated by its GEF BLOC-3. Whether cleaved Rab32 can interact with BLOC-3 has yet to be elucidated. BLOC-3 belongs to heterodimeric RabGEF complexes and exhibits similarities with the Mon1-Ccz1 complex. Therefore, BLOC-3 probably utilizes the same mechanism for the nucleotide exchange as the Mon1-Ccz1 complex does (Nordmann et al., 2010; Kiontke et al., 2017). Furthermore, Rab32 possesses an R55 matching with the K38 of Ypt7, which is crucial for its interaction with Mon1-Ccz1 (Kiontke et al., 2017). As our results show that cleaved switch I has higher flexibility and is dislocated, it would not be surprising if proteolytically modified Rab32 cannot be activated by BLOC-3. Therefore, GtgE-mediated proteolysis may possibly ensure the complete removal of Rab32 by GDI from the SCV membrane enabling the survival of the bacteria within the host cell (Spanò and Galán, 2012; Hu et al., 2019). Interestingly, HeLa cells have a similar copy number of Rab32 and GDI (Itzhak et al., 2016). Thus, an additional effect of $Rab32_{cleaved}$:GDP and $Rab32_{cleaved}$:GppNHp may be a GDI depletion from the host cell securing the higher membrane localization of other Rab GTPases. Furthermore, the proteolytic constitutive deactivation of Rab32 may explain the impairment of itaconate delivery into the SCVs in a Rab32-BLOC3-dependent manner (Chen et al., 2020).

GtgE targets also the Rab32 homolog Rab29 and proteolyzes its switch I between G41 and V42, which is comparable to the cleavage site in Rab32 (Spanò et al., 2011). Moreover, Rab29 interacts with the Armadillo domain of leucine-reach repeat kinase 2 (LRRK2) (McGrath et al., 2019). The result of this interaction is LRRK2 recruitment and activation on the Golgi (Purlyte et al., 2018). Noteworthy is also the activation of the NLRC4 inflammasome by active LRRK2 during *Salmonella* infection (Liu et al., 2017). Therefore, it would be of great interest to investigate whether Rab29 proteolysis by GtgE may impair the Rab29-mediated LRRK2 recruitment and activation on the Golgi, and reduce the activation of NLRC4 inflammasome (Liu et al., 2017; Purlyte et al., 2018). It would also be beneficial to understand whether the kinase activity of LRRK2 during the infection is associated with Rab32 and plays a pivotal role in the defense mechanism of the host against *Salmonella* (Gardet et al., 2010; Liu et al., 2017).

In this study, we demonstrate that the high flexibility and dislocation of switch I, the alteration of the interswitch region, and locking of Rab32 in a GDP-like state by GtgE-mediated cleavage are responsible for impairing the interaction between VARP-ANK1 and Rab32 as well as for binding of GDI to $Rab32_{cleaved}$:GDP or $Rab32_{cleaved}$:GppNHp. These findings expand our understanding about the consequences of GtgE-mediated proteolysis on Rab32, which facilitates *Salmonella* infection. Withal, we provide possible further downstream effects of proteolytic modification of Rab32 and deepen the knowledge about mechanisms of *Salmonella* infection.

Limitations of the study

Results of this study provide a comprehensive insight into the consequences of proteolytic modification of Rab32. However, the ability of cleaved Rab32 to interact with its physiological GEF BLOC-3 and, thereby, be activated remains speculative. In addition, the physiological consequences of the observed *in vitro* effects of Rab32 cleavage will require further elucidation.

Resource availability

Lead contact

Further information and requests for resources and reagents should be directed to and will be fulfilled by Aymelt Itzen (a.itzen@uke.de).

Materials availability

All unique materials generated in this study are available from the Lead Contact without restriction.

Data and code availability

This study did not generate or analyze datasets or code.

Methods

All methods can be found in the accompanying Transparent methods supplemental file.

Supplemental information

Supplemental Information can be found online at https://doi.org/10.1016/j.isci.2020.101940.

Author contributions

S.S., R.W., V.T., D.P.-D., and H.-S.K. performed the experiments. S.S. and R.W. generated all proteins, conducted biochemical and biophysical experiments, and analyzed the data. V.T. performed protein labeling and FRET measurements with subsequent data analysis. D.P.D. performed all MD simulations and helped with data interpretation. H.-S.K. recorded and analyzed HSQC NMR spectra. D.C.L., M.Z., and M.S. contributed to the study with their expertise, guidance, and laboratory equipment. A.I. designed the study and provided oversight of the project, data analysis, and data interpretation. S.S., R.W., and A.I. wrote the manuscript. All authors participated in manuscript editing and final approval.

Declaration of interests

The authors declare no competing interest.

References

Alto, N.M., Soderling, J., and Scott, J.D. (2002). Rab32 is an A-kinase anchoring protein and participates in mitochondrial dynamics. J. Cell Biol. *158*, 659–668.

Ao, X., Zou, L., and Wu, Y. (2014). Regulation of autophagy by the Rab GTPase network. Cell Death Differ. *21*, 348–358.

Barthelmes, K., Ramcke, E., Kang, H.-S., Sattler, M., and Itzen, A. (2020). Conformational control of small GTPases by AMPylation. Proc. Natl. Acad. Sci. U S A *117*, 5772–5781.

Benado, A., Nasagi-Atiya, Y., and Sagi-Eisenberg, R. (2009). Protein trafficking in immune cells. Immunobiology *214*, 507–525.

Biancucci, M., Minasov, G., Banerjee, A., Herrera, A., Woida, P.J., Kieffer, M.B., Bindu, L., Abreu-Blanco, M., Anderson, W.F., Gaponenko, V., et al. (2018). The bacterial Ras/Rap1 site-specific endopeptidase RRSP cleaves Ras through an atypical mechanism to disrupt Ras-ERK signaling. Sci. Signal. *11*, eaat8335.

Bucci, C., Thomsen, P., Nicoziani, P., McCarthy, J., and van Deurs, B. (2000). Rab7: a key to lysosome biogenesis. Mol. Biol. Cell *11*, 467–480.

Bultema, J.J., Ambrosio, A.L., Burek, C.L., and Di Pietro, S.M. (2012). BLOC-2, AP-3, and AP-1 proteins function in concert with Rab38 and Rab32 proteins to mediate protein trafficking to lysosome-related organelles. J. Biol. Chem. *287*, 19550–19563.

Chen, M., Sun, H., Boot, M., Shao, L., Chang, S.-J., Wang, W., Lam, T.T., Lara-Tejero, M., Rego, E.H., and Galán, J.E. (2020). Itaconate is an effector of a Rab GTPase cell-autonomous host defense pathway against Salmonella. Science *369*, 450–455.

Crum-Cianflone, N.F. (2008). Salmonellosis and the gastrointestinal tract: more than just peanut butter. Curr. Gastroenterol. Rep. *10*, 424–431.

Eathiraj, S., Mishra, A., Prekeris, R., and Lambright, D.G. (2006). Structural basis for Rab11-mediated recruitment of FIP3 to recycling endosomes. J. Mol. Biol. *364*, 121–135.

Eathiraj, S., Pan, X., Ritacco, C., and Lambright, D.G. (2005). Structural basis of family-wide Rab GTPase recognition by rabenosyn-5. Nature *436*, 415–419.

Gardet, A., Benita, Y., Li, C., Sands, B.E., Ballester, I., Stevens, C., Korzenik, J.R., Rioux, J.D., Daly, M.J., Xavier, R.J., et al. (2010). LRRK2 is involved in the IFN-gamma response and host response to pathogens. J. Immunol. *185*, 5577–5585.

Gerondopoulos, A., Langemeyer, L., Liang, J.-R., Linford, A., and Barr, F.A. (2012). BLOC-3 mutated in Hermansky-Pudlak syndrome is a Rab32/38 guanine nucleotide exchange factor. Curr. Biol. *22*, 2135–2139.

Goody, P.R., Heller, K., Oesterlin, L.K., Müller, M.P., Itzen, A., and Goody, R.S. (2012). Reversible phosphocholination of Rab proteins by Legionella pneumophila effector proteins. EMBO J. *31*, 1774–1784.

Haile, Y., Deng, X., Ortiz-Sandoval, C., Tahbaz, N., Janowicz, A., Lu, J.-Q., Kerr, B.J., Gutowski, N.J., Holley, J.E., Eggleton, P., et al. (2017). Rab32

connects ER stress to mitochondrial defects in multiple sclerosis. J. Neuroinflammation 14, 19.

Hesketh, G.G., Pérez-Dorado, I., Jackson, L.P., Wartosch, L., Schäfer, I.B., Gray, S.R., McCoy, A.J., Zeldin, O.B., Garman, E.F., Harbour, M.E., et al. (2014). VARP is recruited on to endosomes by direct interaction with retromer, where together they function in export to the cell surface. Dev. Cell 29, 591–606.

Holt, O.J., Gallo, F., and Griffiths, G.M. (2006). Regulating secretory lysosomes. J. Biochem. 140, 7–12.

Hu, Z.-Q., Rao, C.-L., Tang, M.-L., Zhang, Y., Lu, X.-X., Chen, J.-G., Mao, C., Deng, L., Li, Q., and Mao, X.-H. (2019). Rab32 GTPase, as a direct target of miR-30b/c, controls the intracellular survival of Burkholderia pseudomallei by regulating phagosome maturation. PLoS Pathog. 15, e1007879.

Itzhak, D.N., Tyanova, S., Cox, J., and Borner, G.H. (2016). Global, quantitative and dynamic mapping of protein subcellular localization. Elife 5, e16950.

Jagoe, W.N., Lindsay, A.J., Read, R.J., McCoy, A.J., McCaffrey, M.W., and Khan, A.R. (2006). Crystal structure of rab11 in complex with rab11 family interacting protein 2. Structure 14, 1273–1283.

Joberty, G., Tavitian, A., and Zahraoui, A. (1993). Isoprenylation of Rab proteins possessing a C-terminal CaaX motif. FEBS Lett. 330, 323–328.

Kalinin, S., Peulen, T., Sindbert, S., Rothwell, P.J., Berger, S., Restle, T., Goody, R.S., Gohlke, H., and Seidel, C.A.M. (2012). A toolkit and benchmark study for FRET-restrained high-precision structural modeling. Nat. Methods 9, 1218–1225.

Kiontke, S., Langemeyer, L., Kuhlee, A., Schuback, S., Raunser, S., Ungermann, C., and Kümmel, D. (2017). Architecture and mechanism of the late endosomal Rab7-like Ypt7 guanine nucleotide exchange factor complex Mon1-Ccz1. Nat. Commun. 8, 14034.

LeBlanc, S.J., Kulkarni, P., and Weninger, K.R. (2018). Single molecule FRET: a powerful tool to study intrinsically disordered proteins. Biomolecules 8, 140.

Levin, R.S., Hertz, N.T., Burlingame, A.L., Shokat, K.M., and Mukherjee, S. (2016). Innate immunity kinase TAK1 phosphorylates Rab1 on a hotspot for posttranslational modifications by host and pathogen. Proc. Natl. Acad. Sci. U S A 113, E4776–E4783.

Liu, W., Liu, X.'.n, Li, Y., Zhao, J., Liu, Z., Hu, Z., Wang, Y., Yao, Y., Miller, A.W., Su, B., et al. (2017). LRRK2 promotes the activation of NLRC4 inflammasome during Salmonella Typhimurium infection. J. Exp. Med. 214, 3051–3066.

Marubashi, S., Shimada, H., Fukuda, M., and Ohbayashi, N. (2016). RUTBC1 functions as a GTPase-activating protein for rab32/38 and regulates melanogenic enzyme trafficking in melanocytes. J. Biol. Chem. 291, 1427–1440.

McGrath, E., Waschbüsch, D., Baker, B.M., and Khan, A.R. (2019). LRRK2 binds to the Rab32 subfamily in a GTP-dependent manner via its armadillo domain. Small GTPases, 1–14.

Milburn, M.V., Tong, L., deVos, A.M., Brünger, A., Yamaizumi, Z., Nishimura, S., and Kim, S.H. (1990). Molecular switch for signal transduction: structural differences between active and inactive forms of protooncogenic ras proteins. Science 247, 939–945.

Müller, M.P., and Goody, R.S. (2018). Molecular control of Rab activity by GEFs, GAPs and GDI. Small GTPases 9, 5–21.

Müller, M.P., Peters, H., Blümer, J., Blankenfeldt, W., Goody, R.S., and Itzen, A. (2010). The Legionella effector protein DrrA AMPylates the membrane traffic regulator Rab1b. Science 329, 946–949.

Nordmann, M., Cabrera, M., Perz, A., Bröcker, C., Ostrowicz, C., Engelbrecht-Vandré, S., and Ungermann, C. (2010). The Mon1-Ccz1 complex is the GEF of the late endosomal Rab7 homolog Ypt7. Curr. Biol. 20, 1654–1659.

Nottingham, R.M., Ganley, I.G., Barr, F.A., Lambright, D.G., and Pfeffer, S.R. (2011). RUTBC1 protein, a Rab9A effector that activates GTP hydrolysis by Rab32 and Rab33B proteins. J. Biol. Chem. 286, 33213–33222.

Oesterlin, L.K., Goody, R.S., and Itzen, A. (2012). Posttranslational modifications of Rab proteins cause effective displacement of GDP dissociation inhibitor. Proc. Natl. Acad. Sci. U S A 109, 5621–5626.

Pai, E.F., Kabsch, W., Krengel, U., Holmes, K.C., John, J., and Wittinghofer, A. (1989). Structure of the guanine-nucleotide-binding domain of the Ha-ras oncogene product p21 in the triphosphate conformation. Nature 341, 209–214.

Purlyte, E., Dhekne, H.S., Sarhan, A.R., Gomez, R., Lis, P., Wightman, M., Martinez, T.N., Tonelli, F., Pfeffer, S.R., and Alessi, D.R. (2018). Rab29 activation of the Parkinson's disease-associated LRRK2 kinase. EMBO J. 37, 1–18.

Pylypenko, O., Rak, A., Durek, T., Kushnir, S., Dursina, B.E., Thomae, N.H., Constantinescu, A.T., Brunsveld, L., Watzke, A., Waldmann, H., et al. (2006). Structure of doubly prenylated Ypt1:GDI complex and the mechanism of GDI-mediated Rab recycling. EMBO J. 25, 13–23.

Raposo, G., and Marks, M.S. (2007). Melanosomes–dark organelles enlighten endosomal membrane transport. Nat. Rev. Mol. Cell Biol. 8, 786–797.

Raposo, G., Tenza, D., Murphy, D.M., Berson, J.F., and Marks, M.S. (2001). Distinct protein sorting and localization to premelanosomes, melanosomes, and lysosomes in pigmented melanocytic cells. J. Cell Biol. 152, 809–824.

Rybnicek, J., Samtleben, S., Herrera-Cruz, M.S., and Simmen, T. (2018). Expression of a T39N mutant Rab32 protein arrests mitochondria movement within neurites of differentiated SH-SY5Y cells. Small GTPases, 1–4.

Sasaki, T., Kikuchi, A., Araki, S., Hata, Y., Isomura, M., Kuroda, S., and Takai, Y. (1990). Purification and characterization from bovine brain cytosol of a protein that inhibits the dissociation of GDP from and the subsequent binding of GTP to smg p25A, a ras p21-like GTP-binding protein. J. Biol. Chem. 265, 2333–2337.

Scheidig, A.J., Burmester, C., and Goody, R.S. (1999). The pre-hydrolysis state of p21ras in complex with GTP: new insights into the role of water molecules in the GTP hydrolysis reaction of ras-like proteins. Structure 7, 1311–1324.

Spanò, S., and Galán, J.E. (2012). A Rab32-dependent pathway contributes to Salmonella typhi host restriction. Science 338, 960–963.

Spanò, S., Gao, X., Hannemann, S., Lara-Tejero, M., and Galán, J.E. (2016). A bacterial pathogen targets a host rab-family GTPase defense pathway with a GAP. Cell Host Microbe 19, 216–226.

Spanò, S., Liu, X., and Galán, J.E. (2011). Proteolytic targeting of Rab29 by an effector protein distinguishes the intracellular compartments of human-adapted and broad-host Salmonella. Proc. Natl. Acad. Sci. U S A 108, 18418–18423.

Tamura, K., Ohbayashi, N., Ishibashi, K., and Fukuda, M. (2011). Structure-function analysis of VPS9-ankyrin-repeat protein (Varp) in the trafficking of tyrosinase-related protein 1 in melanocytes. J. Biol. Chem. 286, 7507–7521.

Tamura, K., Ohbayashi, N., Maruta, Y., Kanno, E., Itoh, T., and Fukuda, M. (2009). Varp is a novel Rab32/38-binding protein that regulates Tyrp1 trafficking in melanocytes. Mol. Biol. Cell 20, 2900–2908.

Vetter, I.R., and Wittinghofer, A. (2001). The guanine nucleotide-binding switch in three dimensions. Science 294, 1299–1304.

Wachtel, R., Bräuning, B., Mader, S.L., Ecker, F., Kaila, V.R.I., Groll, M., and Itzen, A. (2018). The protease GtgE from Salmonella exclusively targets inactive Rab GTPases. Nat. Commun. 9, 44.

Wasmeier, C., Romao, M., Plowright, L., Bennett, D.C., Raposo, G., and Seabra, M.C. (2006). Rab38 and Rab32 control post-Golgi trafficking of melanogenic enzymes. J. Cell Biol. 175, 271–281.

Wu, M., Wang, T., Loh, E., Hong, W., and Song, H. (2005). Structural basis for recruitment of RILP by small GTPase Rab7. EMBO J. 24, 1491–1501.

Wu, Y.-W., Tan, K.-T., Waldmann, H., Goody, R.S., and Alexandrov, K. (2007). Interaction analysis of prenylated Rab GTPase with Rab escort protein and GDP dissociation inhibitor explains the need for both regulators. Proc. Natl. Acad. Sci. U S A 104, 12294–12299.

Zhu, G., Zhai, P., Liu, J., Terzyan, S., Li, G., and Zhang, X.C. (2004). Structural basis of Rab5-Rabaptin5 interaction in endocytosis. Nat. Struct. Mol. Biol. 11, 975–983.

Supplemental Information

Proteolysis of Rab32

by *Salmonella* GtgE induces

an inactive GTPase conformation

Sergey Savitskiy, Rudolf Wachtel, Danial Pourjafar-Dehkordi, Hyun-Seo Kang, Vanessa Trauschke, Don C. Lamb, Michael Sattler, Martin Zacharias, and Aymelt Itzen
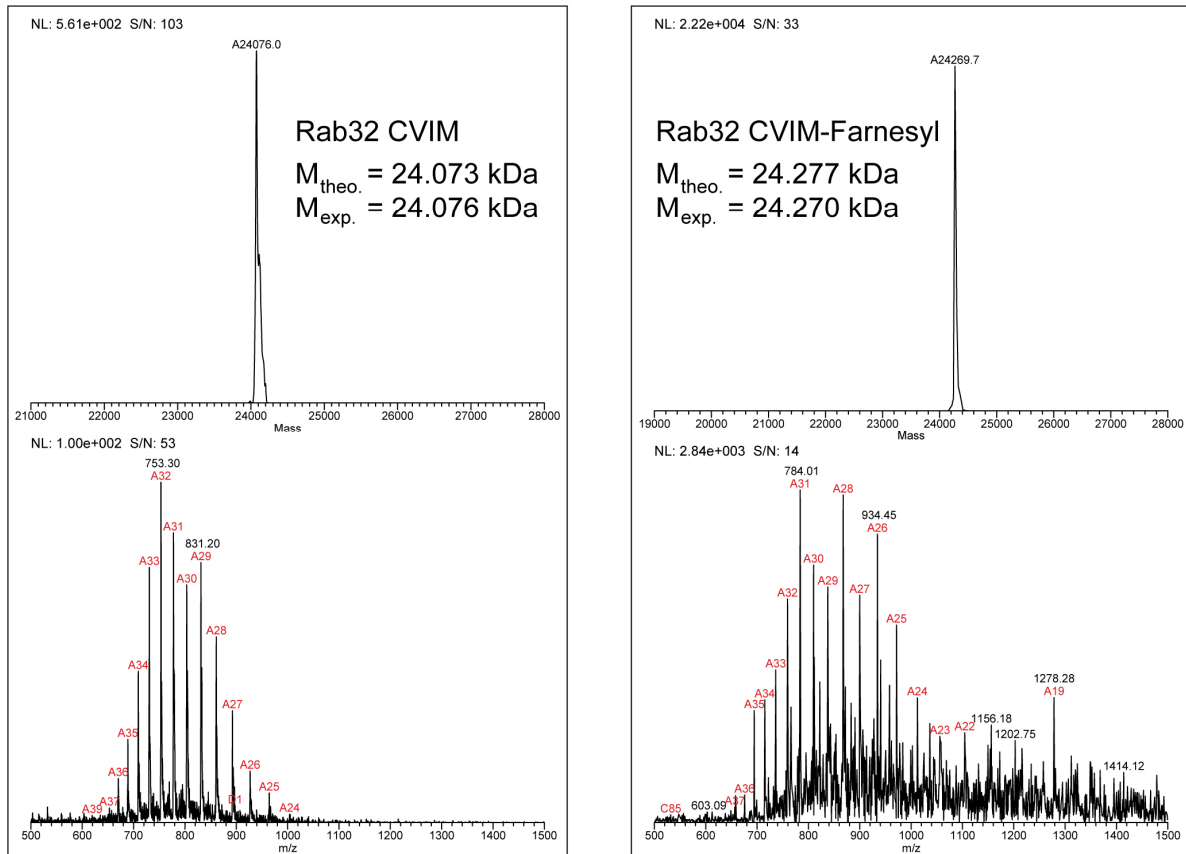
Figure S1: Mass spectrometry data of Rab32 CVIM farnesylation. Related to Figure 2C and 2D. Left: unmodified Rab32 bearing the CVIM-sequence. Right: farnesylated Rab32 CVIM. Both masses were determined with an offset of 3 Da ($M_{exp.}$) compared to the calculated, theoretical mass ($M_{theo.}$) The measured difference in mass ($\Delta M_{exp.}$ = 194 Da) does not correspond fully to the theoretical Mass difference of an attached farnesyl moiety ($\Delta M_{theo.}$ = 204 Da). The difference of 10 Da is due to the mass resolution limitations of the instrument and m/z-data quality of the farnesylated Rab32 which showed significantly less ionization upon modification. The deconvoluted mass spectra (top) and the m/z spectra (bottom) are demonstrated.
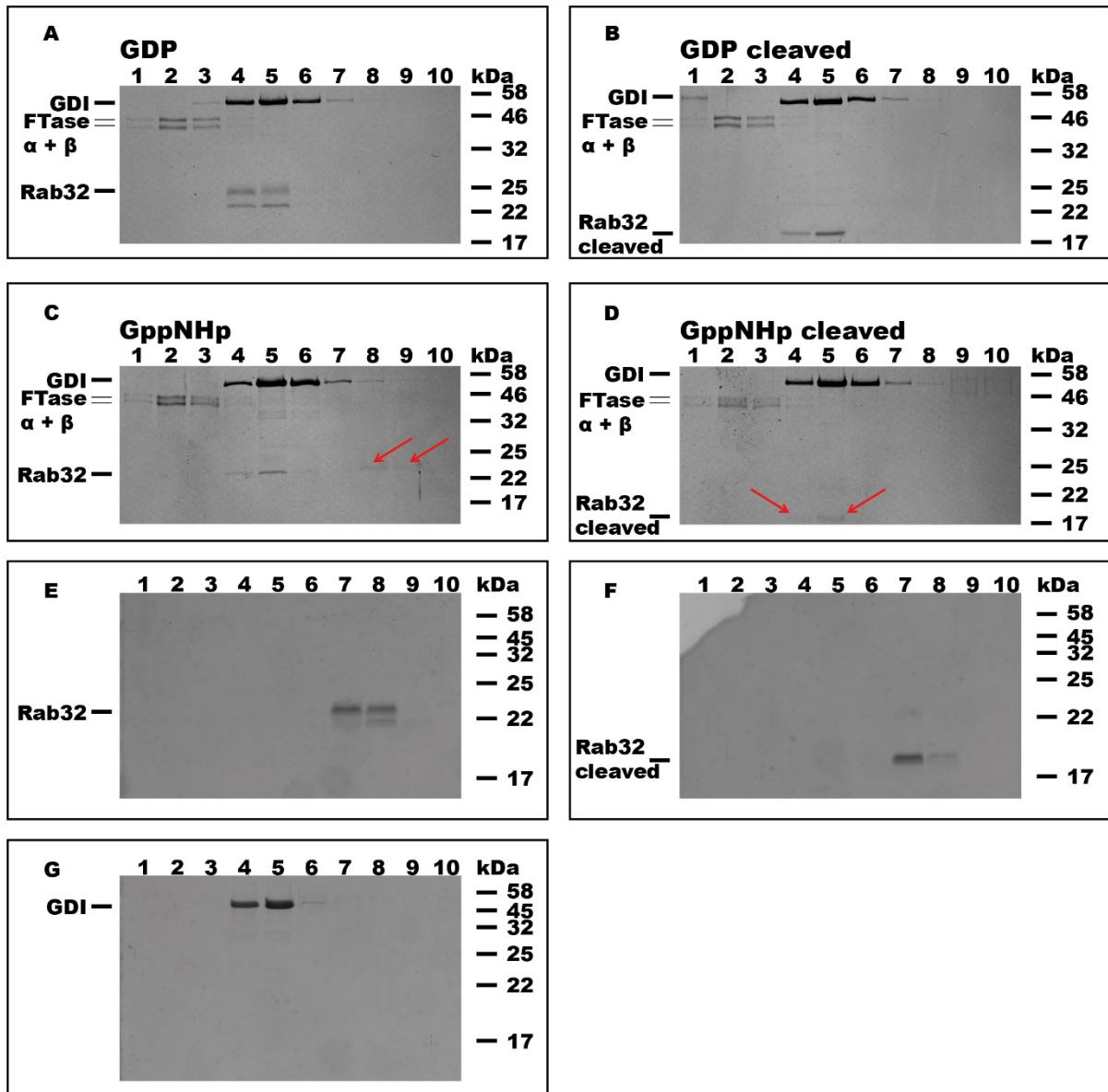
Figure S2: Fraction analysis of the Rab32:GDI complex formation on an aSEC. Related to Figure 2C and 2D. Coomassie stained SDS-PAGE of fractions from aSEC separations containing farnesylated Rab32 CVIM in the presence of GDI and FTase (compare Fig. 2C, 2D). **A** Rab32:GDP. **B** Rab32$_{cleaved}$:GDP. **C** Rab32:GppNHp. **D** Rab32$_{cleaved}$:GppNHp. Slightly visible bands are highlighted with red arrows. All Rab32 preparations (A-D) are forming a non-covalent complex with GDI indicated by the coelution in fractions 4 and 5. Only Rab32:GppNHp (C) shows a partial complex formation indicated by free Rab32 in fractions 8 and 9. **E-G** Control runs of purified proteins (**E**) Rab32, (**F**) Rab32$_{cleaved}$ and (**G**) GDI on an aSEC.
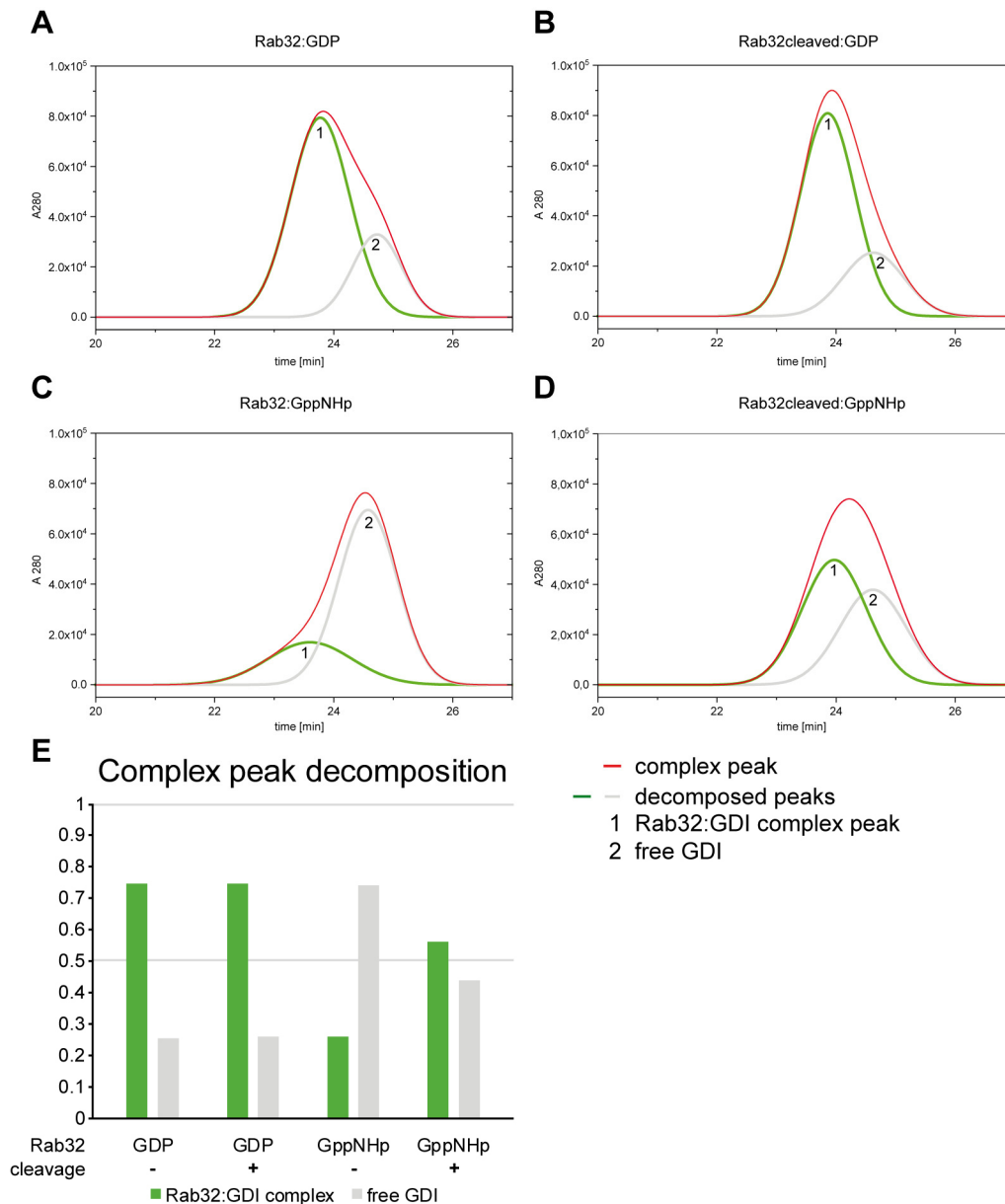
Figure S3: Decomposition of eluted complex peaks of Rab32 and GDI using aSEC. Related to Figure 2C and 2D. (**A**) Rab32:GPD:GDI, (**B**) Rab32$_{cleaved}$:GDP:GDI, (**C**) Rab32:GppNHp:GDI, and (**D**) Rab32$_{cleaved}$:GppNHp:GDI showing both the absorption at 280 nm (red chromatogram) as well as the decomposition of the peak into free GDI (2) and the Rab32:GDI complex (1). Peak decomposition was performed using Origin data analysis software (OriginLab 2019b, v9.65) setting the elution time of free GDI in complex peak to 24.6 min. (**E**) The populations determined in panels A-D are plotted as a bar chart.
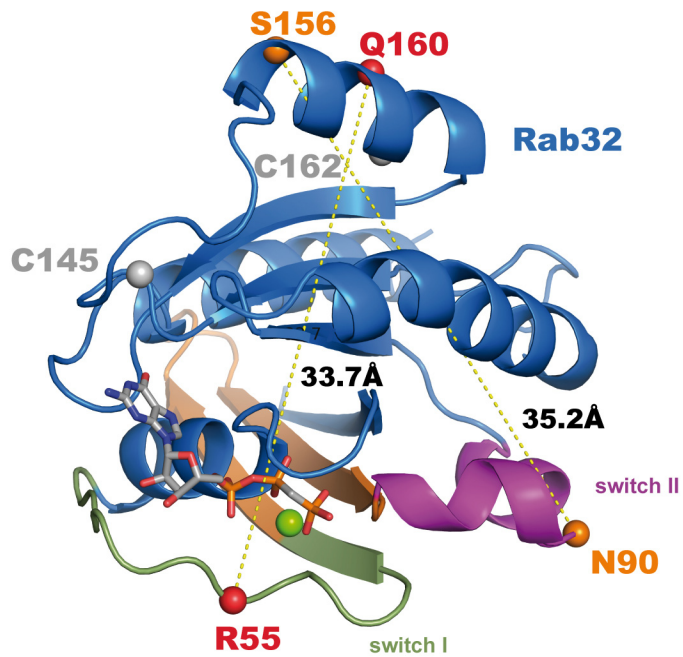
Figure S4: Positions of mutated Cys-residues within the Rab32 structure. Related to Figure 3A. The positions of cysteine mutations and the distances between them are indicated by yellow dotted lines for the two spFRET pairs used (red and orange spheres). Further wild type Cys residues (grey spheres) were mutated to Ser. The positions were labelled stochastically with donor and acceptor molecules. (PDB: 6FF8 (McGrath et al., 2019)).
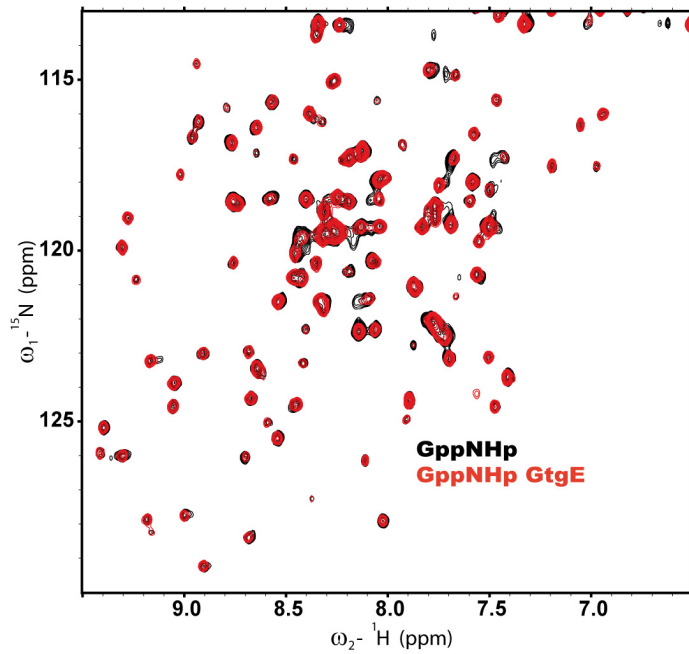
Figure S5: ¹H ¹⁵N HSQC spectra of Rab32:GppNHp with GtgE supplementation. Related to Figure 4. Superimposed spectra of Rab32:GppNHp and Rab32:GppNHp in the presence of GtgE protease are very similar. No significant differences in the signals were observed indicating that nucleotide exchange with GppNHp *in vitro* was already fully completed.

Table S1: Anisotropy data of utilized fluorophores in Rab32 spFRET measurements.
Related to Figure 3C and 3D. Residual fluorescence anisotropy r_{inf} and steady-state fluorescence anisotropy r_{ss} of Alexa488 as the donor and Alexa647 as the acceptor are given.

	Donor only		Acceptor	
Rab32 mutant	r_{inf}	r_{ss}	r_{inf}	r_{ss}
R55C Q160C	0.070	0.081	0.077	0.10
R55C Q160C cleaved	0.085	0.10	0.20	0.29
N90C S156C	0.081	0.12	0.17	0.21
N90C S156C cleaved	0.11	0.12	0.21	0.28

Transparent Methods

Molecular Biology

All cloning procedures were accomplished using the Mach1 *E.coli* strain. Q5® Site-Directed Mutagenesis Kit (KLD, New England Biolabs) was used for generation of all mutants used for this study according to a provided protocol by the manufacturer. The site and ligation independent cloning (SLIC) strategy was applied for generation of all plasmids containing wild type genes used in this study. Rab32 constructs, SopD2 and GtgE were cloned into the pMal™-c2X vector (NEB) with the Factor Xa site replaced by a TEV cleavage site. GDI was cloned into a pFastBacHT A vector for following usage in insect expression system (Oesterlin et al., 2012). Proteins were designed as N-terminal His_6-MBP (and just His_6 with GDI)-fusion proteins. The tags were separated from the gene of interest by a TEV protease cleavage site. Rab32 applied in GDI interaction studies contained CVIM as a C-terminal FTase recognition sequence for prenylation. The VARP gene template was kindly provided by David Owen's Lab (University of Cambridge; (Hesketh et al., 2014)). All further wild type constructs used in this work were generated in a previous study (Wachtel et al., 2018). Oligonucleotides were purchased from Integrated DNA Technologies, Inc. (IDT, Leuven, Belgium). All plasmids were confirmed by Sanger sequencing with Microsynth Seqlab. NCBI accession numbers or Uniprot IDs for the proteins used in this study: Rab32 variants: $Rab32_{1-225}$, $Rab32_{20-201}$, $Rab32_{20-227(CVIM)}$ (NP_006825), $VARP-ANK1_{451-640}$ (NP_115515), GDI_{1-447} (P21856), $SopD2_{1-319}$ (Q8ZQC8), $GtgE_{1-228}$ (A0A0H3N9Y3).

Protein expression

For recombinant production of proteins, the *E. coli* BL21-Codon Plus (DE3) strain (for the Rab32 and the VARP-ANK1 fusion proteins) or BL21-Codon Plus (DE3)-RIL strain (for GtgE and SopD2) were transformed with 100 ng of the respective plasmid and grown overnight in 20 ml of lysogeny broth (LB) medium containing 125 µg/mL ampicillin (and 34 µg/mL chloramphenicol for BL21-Codon Plus (DE3)-RIL cells) at 37°C and 180 rpm (Innova 44 shaking incubator, New Brunswick). The expression cultures (1 L of LB medium or ^{15}N supplemented M9 minimal medium for isotope labelling) containing corresponding antibiotics were inoculated with 20 ml of the overnight cultures and grown under same conditions. At OD_{600} = 0.5-0.8, protein expression was induced by addition of 1 mM isopropylthiogalactopyranosid (IPTG, final) for Rab32 variants and VARP-ANK1 as well as 0.5 mM IPTG for GtgE and SopD2, followed by overnight incubation at 22°C and 180 rpm. GDI was expressed using the baculovirus expression system in *S. frugiperda* cells (Sf9, Thermo Scientific) and was purified as described before (Oesterlin et al., 2012). Cells were harvested by centrifugation at 8500 g and 20°C for 30 min (Sigma 8K, Sigma Centrifuges). After resuspending and washing the pelleted bacteria in phosphate buffered saline (PBS, 137 mM

NaCl, 2.7 mM KCl, 10 mM NaH_2PO_4, 2 mM KH_2PO_4), cells were centrifuged at 3000 g and 4°C for 20 min (5810 R, Eppendorf). The pellets were snap frozen in liquid nitrogen and stored at -20°C until further use.

Protein purification

Pellets containing GtgE, SopD2 or VARP-ANK1 were resuspended in buffer A (50 mM HEPES, 500 mM NaCl, 1 mM $MgCl_2$, 2 mM β-Mercaptoethanol (ß-ME) at pH 7.5 in a ratio of 10 ml buffer to 1 g pellet. For pellets containing Rab32 buffer A was supplemented with 10 µM Guanosine 5′-diphosphate (GDP). A spatula tip of DNAse I (Sigma Aldrich) was added to the suspension and cells were disrupted in a high-pressure fluidizer at 1.8 kbar (Constant Systems Ltd.). Subsequently, 1 mM phenylmethylsulfonylfluorid (PMSF, final concentration) was added and the crude protein extract was cleared by centrifugation at 20000 rpm and 4°C for 45 min (Avanti J-26 XP with JA25.50 rotor, Beckman Coulter). The crude lysate containing VARP-ANK1 was supplemented with 1 mM 4-(2-Aminoethyl)benzenesulfonyl fluoride (AEBSF; Sigma Aldrich, final concentration) and 5% of glycerol (v/v) before clearing the lysate.

For the purification of all proteins via fused His_6-affinity tag, the cleared protein extract was applied to an immobilized metal affinity chromatography (IMAC) using a 5 mL Nuvia column chelating Ni^{2+}-ions (Bio-Rad Laboratories) that was equilibrated with buffer A beforehand. For all chromatography purifications, the NGC Quest™ 10 medium-pressure liquid chromatography (MPLC) system (Bio-Rad) was used. The cleared lysate was loaded onto the column and washed with 6-8 column volumes (CV) 8% buffer B (buffer A supplemented with 500 mM imidazole). Subsequently, a 20 CV gradient of 8-100% buffer B was applied, where target proteins eluted between 18-35% buffer B. Relevant fractions were analyzed by sodium dodecylsulfate polyacrylamide gel electrophoresis (SDS-PAGE) and pure protein fractions were pooled. Subsequently, the proteins were dialyzed against 5 L dialysis buffer (20 mM HEPES, 100 mM NaCl, 2 mM ß-ME at pH 7.5) overnight at 4°C. During dialysis, the target proteins were incubated with 1 mg TEV-protease (containing a His_7-affininty tag, in house preparation) per 40 mg target protein in order to quantitatively cleave the fused His_6-affinity and MBP solubility tag. To purify the proteins of interest from the protease and the cleaved tags, reverse IMAC was applied, either collecting the target protein in the flow through (GtgE, SopD2, and VARP-ANK1) or 5% buffer B elution fraction (Rab32 variants).

For further purification size exclusion chromatography using a 16/600 Superdex 75 pg column (GE Healthcare) was performed. The column was equilibrated with gel filtration buffer (20 mM HEPES, 50 mM NaCl, 1 mM $MgCl_2$, 10 µM GDP, 2 mM DTT at pH 7.5 for Rab32 and the same buffer system without GDP for other proteins). Fractions containing pure and monodispers protein of interest were identified by SDS-PAGE, concentrated to 5-30 mg/mL using Amicon Ultra 15 ml centrifugal filters (Merck Millipore), flash frozen in liquid nitrogen, and stored at -80°C.

GTPase nucleotide loading

The inactive Rab32:GDP variants were prepared by incubation of the crude protein extract with purified, tag-free SopD2 (50 nM) directly after cell disruption for 30 min at room temperature before the first IMAC was performed. The GTP or GppNHp exchange was performed in SEC buffer by supplementing the buffer with 5 mM EDTA and 40-fold excess of the desired nucleotide to a small GTPase and incubated at room temperature for 2 h. Nucleotide exchange was stopped by adding 5 mM $MgCl_2$ (final concentration) to the protein solution and separation of the GTPase from excess of nucleotide was performed using a NAP5 desalting column equilibrated with SEC buffer containing 10 µM GDP or 1 µM GppNHp respectively. Protein containing eluate was confirmed with NanoDrop^{TM} 2000 (Thermo Scientific), flash frozen in liquid nitrogen, and stored at -80°C. Nucleotide loading efficiency was verified by ion-pairing reversed-phase high performance chromatography. To this end, protein samples (40 µM, 22 µL) were heat precipitated at 95°C for 5 min and centrifuged for 5 min at 21000 g. Supernatant was subjected to chromatographic separation on Shimadzu UFPLC (Prominence series) equipped with C18 column (Prontosil C18, F184PS050, Bischoff Chromatography) using 50 mM potassium phosphate buffer pH 6.6, 10 mM tetra-n-butylammonium bromide, 12% acetonitrile (v/v). Nucleotides were detected at 254 nm and resulting peaks were integrated and normalized to the total amount of nucleotides detected set to 100%. The retention time of each nucleotide was determined with the respective nucleotide standard in a separate run.

Rab32 farnesylation

Rab32 was incubated with FTase (in house preparation as described before (Hougland et al., 2012)) in the presence of farnesyl pyrophosphate (FPP, Sigma Aldrich) for 2 h at 30°C and 300 rpm (Rab32:FTase:FPP molar ratio 2:1:12) in the reaction buffer (20 mM HEPES, 50 mM NaCl, 1 mM $MgCl_2$, 0.5 mM $ZnCl_2$, 10 µM GDP, 2 mM DTT at pH 7.5). Farnesylation was confirmed via intact protein mass spectrometry on a LCMS system.

Rab32 proteolysis by GtgE

For quantitative modification, Rab32:GDP was submitted to GtgE-mediated proteolysis at 25°C for 2 h (GtgE:Rab32 molar ratio 1:200) in a gel filtration buffer (20 mM HEPES, 50 mM NaCl, 1 mM $MgCl_2$, 10 µM GDP, 2 mM DTT at pH 7.5). Cleaved Rab32 variants used in spFRET measurements were generated as described recently (Fauser et al., 2020). Proteolysis completion was monitored via SDS-PAGE.

Protein complex formation on analytical size exclusion chromatography

For the complex formation of Rab32 with VARP-ANK1 and GDI a Superdex 75 10/300 GL (GE Healthcare) was attached to a UFPLC system (Prominence series, Shimadzu). For complex formation with VARP, the respective Rab32 preparation was incubated with VARP-ANK1 in a

1:1 molar ratio (50 µM) at 15°C for 1 hour. For GDI binding studies, Rab32 was additionally farnesylated before the incubation with GDI for complex formation (1:1 molar ratio, 50 µM). Subsequently, 50 µl were chromatographically separated on an aSEC and fractionated to 0.5 ml fractions. The gel filtration buffer (20 mM HEPES at pH 7.5, 50 mM NaCl, 1 mM MgCl$_2$, 2 mM DTT, 10 µM GDP or 1 µM GppNHp respectively) was used as a mobile phase for protein separation at 0.5 ml/min flow rate. Proteins were detected at 280 nm. The individual runs of single proteins served as a reference. Vitamin B$_{12}$ was used as an internal standard.

Fluorescent labeling of proteins

The buffer of the proteins was exchanged to 20 mM HEPES, 50 mM NaCl, 1 mM MgCl$_2$, 10 µM GDP at pH 7.5 using a PD MiniTrap G-25 column (GE Healthcare). After concentrating the protein with a Vivaspin 500 10 kDa (Sartorius) spin column, the protein was added to a premixed dye solution (2x molar excess of Alexa488-Maleimide and Alexa647-Maleimide) and incubated at room temperature for 2 h. The remaining free dye was removed using a PD MiniTrap G-25 column and the protein was concentrated using Vivaspin 500 10 kDa (Sartorius) centrifugal filters.

Single-pair FRET measurements

For the spFRET measurements, the Rab32 mutants were diluted to concentrations in the range of 20–100 pM in buffer containing 20 mM HEPES, 50 mM NaCl, 1 mM MgCl$_2$ and 10 µM GDP at pH 7.5. Measurements were carried out on a homebuilt (Barth et al., 2019) three-color dual-polarization confocal microscope with pulsed-interleaved excitation (Kapanidis et al., 2004; Müller et al., 2005) and multi-parameter fluorescence detection (Eggeling et al., 2001) using only two of the laser lines (LDH-D-C-485, LDH-D-C-640, PicoQuant). The laser power measured before the objective were 100 µW for blue excitation and 70 µW for red excitation. Bursts of single molecules diffusing through the confocal volume of the microscope were measured for at least 3 h. The obtained data was analyzed with PAM (Schrimpf et al., 2018), a Matlab-based software. Bursts with a minimum of 100 photons were selected and the ALEX-2CDE filter (Tomov et al., 2012) was used to further narrow down the burst selection to only double-labeled proteins. Single-dye populations were used to calculate crosstalk and direct excitation. The γ-factor was calculated by a linear interpolation of 1/S vs. E of a control measurement of a DNA sample containing two different FRET populations, since the protein measurements mainly showed only one population. Distances were determined using the photon distribution analysis (Antonik et al., 2006) with a Förster radius of 52 Å, which was adjusted from the manufacturers value due to our assumption of n = 1.4 for the index of refraction and the decreased lifetime and thus reduced quantum yield of Alexa488 when labeled to Rab32.

Molecular dynamics simulations

The crystal structure of Rab32 in complex with GppCp and the effector VARP (PDB:4CYM (Hesketh et al., 2014)) served as the starting structure for the molecular dynamics simulations. VARP atoms were removed and the carbon atom between the β- and ɣ-phosphate was replaced with oxygen to replicate GTP. Furthermore, a Mg^{2+} ion was inserted in a position such that it had contact with both the β- and ɣ-phosphate. The gamma phosphate was removed to form the GDP-bound variants of Rab32. The Amber ff14sb force field (Maier et al., 2015) was used for the protein, while additional parameters for GDP and GTP were taken from the Amber parameter database (Meagher et al., 2003). The peptide bond between G59 and V60 was removed to form the proteolized variants of Rab32. Sodium and chloride ions were added to reach a salt concentration of 0.1 M. The complex was set at the center of a truncated octahedron box large enough to have a minimum distance of 10 Å from the edges and filled with water molecules that were modelled using OPC 4-point rigid model (Izadi et al., 2014). The solvated box was then energy minimized (5000 steps), followed by 25 ps of heating and 50 ps of density equilibration, followed by a simulation using an NPT ensemble at 300 K. During these phases, the protein's heavy atoms, the nucleotide and the magnesium ions were restrained at their initial positions using a harmonic potential with a decreasing force constant starting at 5.0 $kcal.mol^{-1}Å^{-2}$ and ending with 1.0 $kcal.mol^{-1}Å^{-2}$. The rest of the simulations were performed without any restraints. The pmemd version of the Amber 16 software package was used employing the hydrogen mass repartitioning feature of the Parmed tool, which allows a simulation time step of 4fs (Case et al., 2016). Long range interactions were included using the particle mesh Ewald (PME) method combined with periodic boundary conditions and a 9 Å cut-off for real space non-bonded interactions. Trajectories were processed and analyzed using CPPTRAJ program. Figures were generated using the PyMol software package (Schrödinger, 2015).

NMR

The uniformly ^{15}N-labeled NMR samples of Rab32 were at 100 µM protein concentration in buffer (20 mM HEPES pH 7.5, 50 mM NaCl, 1 mM $MgCl_2$, 2 mM DTT, 10 µM GDP) with 10% D_2O for a lock signal. NMR experiments were recorded at 298 K on a 600-MHz Bruker Avance NMR spectrometer with cryogenic triple resonance gradient probes. NMR spectra were processed by TOPSPIN3.5 (Bruker), then analyzed using NMRFAM-SPARKY (Lee et al., 2015). Due to the limited sample stability and quantity, our multiple attempts toward signal assignment were not successful.

Circular dichroism

Measurements of CD spectra were carried out on a JASCO 715 CD spectrometer equipped with a Peltier-temperature controller. Spectra were measured at 20 µM protein concentration

in a quartz cuvette with 1 mm path length (Hellma) in 1 mM HEPES pH 7.5, 2.5 mM NaCl, 50 µM $MgCl_2$, 0.5 µM GDP or GppNHp. The temperature was increased by 30°C/h and molar ellipticity was measured at 220 nm. Data were normalized by setting the plateau signal of the thermally unfolded protein to 1.0.

Fluorescence spectroscopy

For determination of the nucleotide dissociation kinetics of Rab32 and Rab32$_{cleaved}$, appropriate GTPase was loaded with GDP or GppNHp (not hydrolysable GTP analogue) bearing a mant fluorescent moiety. The mant-GDP or mant-GppNHp nucleotide dissociation was monitored via the release of the fluorescent nucleotide resulting in a decrease of the fluorescent signal using a fluorescence spectrometer FP-8300 (JASCO) with the following parameters: λ_{exc}: 360 nm, λ_{em}: 440 nm, excitation slit: 1 nm, emission slit: 5 nm. Measurements were conducted at 20°C in 20 mM HEPES, 50 mM NaCl, 1 mM $MgCl_2$, 1 mM ß-ME at pH 7.5 with 500 nM Rab32. Nucleotide exchange was started by addition of an excess of the corresponding mant-free nucleotide (400x) to the Rab32 in the cuvette (Hellma). Full dissociation was achieved by addition of 5 mM EDTA into the cuvette to maximize the nucleotide release.

Determination of mant-nucleotide dissociation rates

For the determination of nucleotide dissociation (k_{off}) measured by fluorescence spectroscopy, reaction curves were fitted to a one-phase exponential decay function with time constant parameter according to equation 1 using the software OriginPro (OriginLab, 2019b, v9.65).

$$F(t) = F_0 + F_A \cdot e^{-t \times k_{off}} \quad \text{equation (1)}$$

with F(t): fluorescence intensity, F_0: minimum fluorescence intensity, F_A: total fluorescence amplitude (i.e. $F_{max} - F_0$, with F_{max}: maximum fluorescence intensity), k_{off}: dissociation constant. Statistical significance was validated by paired Student's t-test in GraphPad Prism (Version 4.0).

Mass spectrometry

All samples for mass spectrometry (MS) analysis were diluted in water to a final protein concentration of 0.1 mg/ml and 1 µl was applied to an ESI-ion trap mass spectrometer (LCQ fleet, Thermo Scientific) coupled to an UHPLC system (Ultimate 3000, Thermo Scientific) equipped with a ProSwift™ RP-4H column (1×50 mm, Thermo Scientific) at a flow rate of 0.2 ml/min. The proteins eluted with a linear gradient of 5–50% acetonitrile (0.1% formic acid) in 6 min. The total ion chromatogram raw data were analyzed with the Xcalibur Software v.3.1 (Thermo Scientific) and deconvoluted using MagTran v.1.02 (Zhang and Marshall, 1998).

References

Antonik, M., Felekyan, S., Gaiduk, A., Seidel, C.A.M., 2006. Separating structural heterogeneities from stochastic variations in fluorescence resonance energy transfer distributions via photon distribution analysis. J Phys Chem B *110*, 6970–6978.

Barth, A., Voith von Voithenberg, L., Lamb, D.C., 2019. Quantitative Single-Molecule Three-Color Förster Resonance Energy Transfer by Photon Distribution Analysis. J Phys Chem B *123*, 6901–6916.

Case, D.A., Betz, R.M., Cerutti, D.S., Cheatham, T.E., III, Darden, T.A., Duke, R.E., Giese, T.J., Gohlke, H., Goetz, A.W., Homeyer, N., Izadi, S., Janowski, P., Kaus, J., Kovalenko, A., Lee, T.S., LeGrand, S., Li, P., Lin, C., Luchko, T., Luo, R., Madej, B., Mermelstein, D., Merz, K.M., Monard, G., Nguyen, H., Nguyen, H.T., Omelyan, I., Onufriev, A., Roe, D.R., Roitberg, A., Sagui, C., Simmerling, C.L., Botello-Smith, W.M., Swails, J., Walker, R.C., Wang, J., Wolf, R.M., Wu, X., Xiao, L. and Kollman, P.A., 2016. AMBER 2016, University of California, San Francisco.

Eggeling, C., Berger, S., Brand, L., Fries, J.R., Schaffer, J., Volkmer, A., Seidel, C.A.M., 2001. Data registration and selective single-molecule analysis using multi-parameter fluorescence detection. Journal of Biotechnology *86*, 163–180.

Fauser, J., Savitskiy, S., Fottner, M., Trauschke, V., Gulen, B., 2020. Sortase-Mediated Quantifiable Enzyme Immobilization on Magnetic Nanoparticles. Bioconjug Chem *31*, 1883–1892.

Hesketh, G.G., Pérez-Dorado, I., Jackson, L.P., Wartosch, L., Schäfer, I.B., Gray, S.R., McCoy, A.J., Zeldin, O.B., Garman, E.F., Harbour, M.E., et al., 2014. VARP is recruited on to endosomes by direct interaction with retromer, where together they function in export to the cell surface. Dev Cell *29*, 591–606.

Hougland, J.L., Gangopadhyay, S.A., Fierke, C.A., 2012. Expansion of protein farnesyltransferase specificity using "tunable" active site interactions: development of bioengineered prenylation pathways. J Biol Chem *287*, 38090–38100.

Izadi, S., Anandakrishnan, R., Onufriev, A.V., 2014. Building Water Models: A Different Approach. J Phys Chem Lett *5*, 3863–3871.

Kapanidis, A.N., Lee, N.K., Laurence, T.A., Doose, S., Margeat, E., Weiss, S., 2004. Fluorescence-aided molecule sorting: analysis of structure and interactions by alternating-laser excitation of single molecules. Proc Natl Acad Sci U S A *101*, 8936–8941.

Lee, W., Tonelli, M., Markley, J.L., 2015. NMRFAM-SPARKY: enhanced software for biomolecular NMR spectroscopy. Bioinformatics *31*, 1325–1327.

Maier, J.A., Martinez, C., Kasavajhala, K., Wickstrom, L., Hauser, K.E., Simmerling, C., 2015. ff14SB: Improving the Accuracy of Protein Side Chain and Backbone Parameters from ff99SB. J Chem Theory Comput *11*, 3696–3713.

McGrath, E., Waschbüsch, D., Baker, B.M., Khan, A.R., 2019. LRRK2 binds to the Rab32 subfamily in a GTP-dependent manner via its armadillo domain. Small GTPases, 1–14.

Meagher, K.L., Redman, L.T., Carlson, H.A., 2003. Development of polyphosphate parameters for use with the AMBER force field. J Comput Chem *24*, 1016–1025.

Müller, B.K., Zaychikov, E., Bräuchle, C., Lamb, D.C., 2005. Pulsed interleaved excitation. Biophys J *89*, 3508–3522.

Oesterlin, L.K., Goody, R.S., Itzen, A., 2012. Posttranslational modifications of Rab proteins cause effective displacement of GDP dissociation inhibitor. Proc Natl Acad Sci U S A *109*, 5621–5626.

Schrimpf, W., Barth, A., Hendrix, J., Lamb, D.C., 2018. PAM: A Framework for Integrated Analysis of Imaging, Single-Molecule, and Ensemble Fluorescence Data. Biophys J *114*, 1518–1528.

Schrödinger, 2015. LLC, The PyMOL Molecular Graphics System, Version 2.0.

Tomov, T.E., Tsukanov, R., Masoud, R., Liber, M., Plavner, N., Nir, E., 2012. Disentangling subpopulations in single-molecule FRET and ALEX experiments with photon distribution analysis. Biophys J *102*, 1163–1173.

Wachtel, R., Bräuning, B., Mader, S.L., Ecker, F., Kaila, V.R.I., Groll, M., Itzen, A., 2018. The protease GtgE from Salmonella exclusively targets inactive Rab GTPases. Nat Commun *9*, 44.

Zhang, Z., Marshall, A.G., 1998. A universal algorithm for fast and automated charge state deconvolution of electrospray mass-to-charge ratio spectra. J Am Soc Mass Spectrom *9*, 225–233.